I&EC research
Industrial & Engineering Chemistry Research
pubs.acs.org/IECR
Review

Advances in Melt Blowing Process Simulations

Joseph Schmidt,[§] Saurabh Shenvi Usgaonkar,[§] Satish Kumar, Karen Lozano,* and Christopher J. Ellison*

Cite This: *Ind. Eng. Chem. Res.* 2022, 61, 65−85

ABSTRACT: Melt blowing is a widely used process for manufacturing nonwoven fiber products with applications spanning healthcare, agriculture, transportation, and infrastructure, among others. The process includes extrusion of a polymer melt through orifices, drawing fiber using high-speed air jets, solidification by cooling with entrained ambient air, and collection in the form of a fiber mat. The structural features and properties of the final mat are determined by a complex interplay between materials selection and fiber dynamics, air flow, and temperature characteristics from die to collector. For the latter, both process variable values and geometrical factors have substantial influence. Many experimental investigations have advanced fundamental understanding in this area, but these studies are challenging due to high air velocities, high temperatures, and the often space-constrained nature of the process, especially near the die exit. Such complexities have sparked significant interest in developing mathematical models and using computer simulations to reveal deeper fundamental insights. Herein, we review advances in melt blowing simulations by presenting employed methods and key findings in the area. We finish by describing some challenges and opportunities for further research.

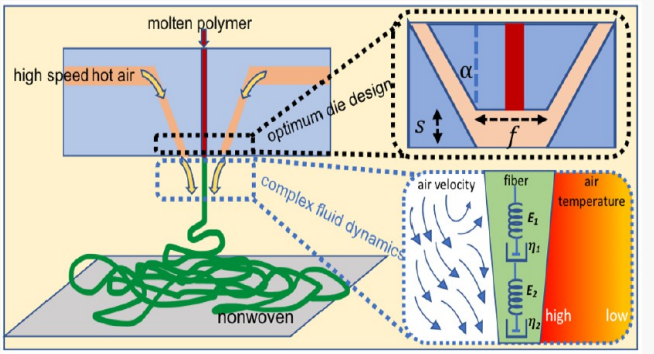

OVERVIEW

The Melt Blowing Process. Melt blowing is a fiber manufacturing process that combines high-temperature, high-velocity air jets, and polymer melts for creating nonwoven fine fiber mats. The process is described schematically in Figure 1 which begins with a solid polymer (pellets, granules, chips, or powder) being melted and extruded into a die at a controlled flow rate. Inside the die is a melt feed system that distributes the melt through orifices usually arranged in a linear fashion; orifices that are 250−500 μm in diameter are typically spaced at 1−4 orifices per millimeter.[1]

Upon exiting the die, the polymeric filaments extruded at rates of 0.3−3 g/hole/min encounter high-temperature (230−360 °C), high-velocity air (typically near or below the speed of sound), with the melt and air flow rates adjusted to produce desired fiber diameters.[2−4] Commercial melt blowing processes have reported use of polymers with melt flow rate (MFR) up to 1500; MFR is a standardized metric related to the polymer viscosity.[5] The hot air jets produce a frictional drag force on the fiber surface that stretches or draws the fibers to smaller diameters (Figure 2).[6,7] During the process, a significant amount of polymer chain stretching and alignment can take place. It is noteworthy that the fiber path below the die becomes chaotic with a significant amount of whipping resulting in drag contributions from the air flow, both axially and transverse to the fibers' long axis. Throughout this article, we use the term "jet" to refer to the air stream(s) in the melt blowing process.

Further away from the die face, the air jets entrain ambient air that cools the fiber causing it to solidify by crystallization and/or vitrification. The solid fibers, with a typical average fiber diameter greater than 1 μm, are then placed onto a moving porous substrate, called a collector plate, typically located 10−50 cm away from the die face,[8−10] often using a vacuum source on the backside of the substrate to pull the fibers onto it.[11] This process, called "laydown", is crucial in defining the final product properties of the entangled, randomly oriented fibers in a mat, called the nonwoven. Some major advantages of the melt blowing process are its high throughput and solventless nature, the ability to tune the final fiber properties by varying process variables, and the availability of a wide range of compatible polymers.[12]

Even though several commercial processes have reported the mean final fiber diameter between 1 and 5 μm,[5,13] efforts have been directed toward fabricating submicron-sized fibers using melt blowing.[14] The produced nonwovens have significant

Received: August 25, 2021
Revised: October 29, 2021
Accepted: November 5, 2021
Published: December 20, 2021

https://doi.org/10.1021/acs.iecr.1c03444
Ind. Eng. Chem. Res. 2022, 61, 65−85

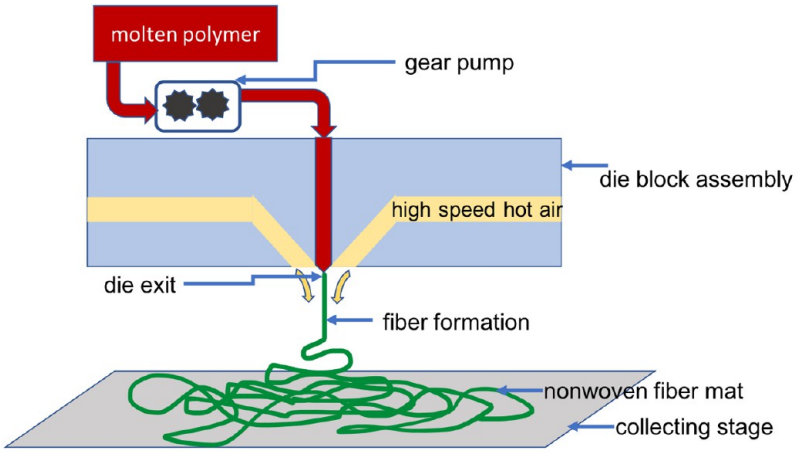

Figure 1. Schematic of the melt blowing process.

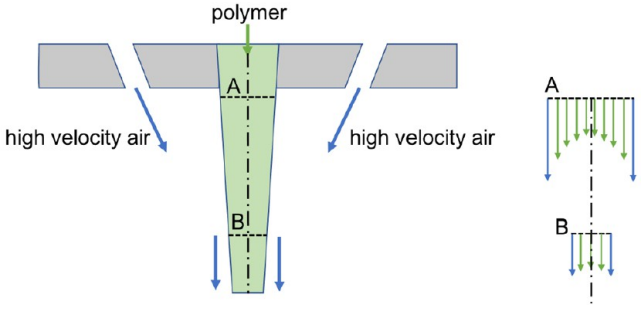

Figure 2. Schematic of the fiber attenuation process after exiting the die (shown on the left) and the velocity profiles of the air (blue) and polymer (green) at points A and B (shown on the right).

porosity and a unique entangled architecture which is useful for applications in a variety of industries.[15] For example, nonwovens have been widely adopted for fine-particle filtration required in gas and liquid filters, and garments and masks for medical personnel and general consumers. Other promising potential applications, including use in transportation, pharmaceutical, energy, and smart textiles, are gaining momentum.[15]

History and Motivation for Simulations. The idea of producing nonwoven microfibers was introduced in 1939 when Carlton Francis envisioned a spray gun that would dispense fibers.[16] Research was undertaken in the 1940s and 1950s; but many challenges were encountered, and unexpected results stalled advancement.[17] In 1954, Van A. Wente created fibers in the order of 10 μm using melt blowing techniques, and Esso (now ExxonMobil) continued research in this area in the 1960s, garnering several patents and improving the production output of nonwoven textiles using thermoplastics.[16] Esso used precise manufacturing techniques to make dies and feed systems that would maximize production capabilities while minimizing prevalent defects such as shot (globular fragments of fibers). Since 1970, significant research has led to more than 560 patents that detail improvements in polymer feed systems, die geometries, air flow turbulence reduction, and other aspects of the melt blowing process.[8,17]

Understanding the complex interplay between various physical processes and instrument geometries in the melt blowing process is a major challenge in attaining controlled fiber diameters. For instance, the air velocity close to the die plays a major role in determining the final fiber diameter and its distribution. The difficulty in measuring this air velocity without disrupting the air flow poses a major challenge for process development. Moreover, the complex interplay between various input parameters like temperature, air velocity, flow rates, and polymer melt viscosity affecting the final fiber quality further complicates the development of a unified framework for understanding and optimizing the melt blowing process. Experimentally exploring the vast available parameter space is difficult. These complexities have motivated the use of computer simulations for building model systems that can mimic the melt blowing process and promote a better understanding of the factors that affect final fiber properties.

The complex nature of the turbulent air flow associated with melt blowing lends itself to computational fluid dynamics (CFD) simulations. Three-dimensional (3D) CFD modeling has allowed for testing of numerous novel die designs by allowing determination of temperature or velocity field close to the die face before experimentation.[18,19] Other models describing the fluid flow associated with the feed distribution system and fiber dynamics can be implemented quickly with low computing cost allowing for greater exploration of design parameters.[2] In most cases, the model predictions agree reasonably well with experiments. Simulations prove to be a powerful tool that can help design experiments and explore the parameter space with the ultimate goal of achieving desired fiber properties.

In this review, we present an overview of the simulations used to understand various aspects of the melt blowing process. We begin by describing CFD of the airfield after it exits the die. Proceeding to standalone fiber simulations, we report on the use of different models to mimic fiber behavior in air flow fields. Combining air and fiber simulations gives insights into the interactions between the air flow field and fiber, thus promoting a deeper understanding of fiber mat qualities, such as porosity and entanglements. Later, we describe simulations of polymer feed distribution approaches for creating uniform fibers on a large scale and how the material properties may affect the final fiber characteristics. Finally, we conclude by identifying some challenges in simulating the melt blowing process and suggest a few specific areas for future research.

https://doi.org/10.1021/acs.iecr.1c03444
Ind. Eng. Chem. Res. 2022, 61, 65−85

AIR FLOW SIMULATIONS

Setting up the Simulation Domain. For simulations to qualitatively and quantitatively represent experiments, setting up an accurate computational domain while observing the limitations of computational resources is required. For example, simulations in 2D agree closely with experimental measurements and prove suitable for studying basic turbulence qualities of the air flow,[2,20] while requiring less computational resources compared to 3D simulations. Moreover, the use of rotational and planar symmetries allows for a reduction in the computational domain size.

Simulations in 2D reveal that a sharp air velocity decay occurs near the die exit, while the air temperature decay occurs further from the die,[21] results that compare well with experiments, thus allowing for air flow or temperature to be simulated using simplified air flow models and smaller domains. Implementing empirical correlations for lateral velocities to introduce eddy currents and turbulence can yield faster results and a more realistic representation of the process without requiring computationally expensive techniques.[7,18] Similarly, boundary conditions at the die inlet need to be modeled, and many approaches assume that the die walls are perfect insulators to simplify the computations.[2] Simplified assumptions can also be made about the temperature dependence of polymer viscosity and the insulating properties of the air to provide basic insights into the process, but careful assessment of such simplifications is required.

To the best of our knowledge, 3D simulations perform better than 2D versions in the following scenarios: 1) to capture and study the whipping amplitude of fiber more accurately, even though 3D simulations underpredict the whipping amplitude as compared to experimental measurements,[22] and 2) to study the integral laydown properties of nonwovens, like the porosity, permeability, and three-dimensional microstructure.[8] Intuitively, a tradeoff is that 3D simulations usually prove much more computationally expensive than 1D or 2D simulations.

CFD is often used to simulate the entire domain to compare far-field results to instrumental readings and extrapolate properties to near the die where experimental measurements are difficult. A critical region is within 1 cm of the die exit where fiber attenuation is most affected by temperature fluctuations.[2] CFD can simulate regions near the die to understand factors that affect fiber formation but at an increased computational cost due to finer meshing requirements. Another common simplification used to reduce computational complexity is to neglect the presence of polymer fibers in the air stream. However, this does not allow the interplay between the air flow field and fiber to be captured which may be central to developing more thorough insights into the fiber formation process.[2]

Different Turbulence Models. Besides setting up the simulation domain, there is also a challenge in selecting the appropriate turbulence model for the air flow field. ANSYS, a commercial software generally used for air flow field simulations, offers three major turbulence models: Direct Numerical Simulation, Scale Resolving Simulation, and Reynolds-Averaged Navier–Stokes in order of decreasing computational expense but decreasing spatial resolution (as shown in Figure 3). Reynolds-Averaged Navier–Stokes models are commonly used in melt blowing research and will be the major focus here, with brief descriptions of the others.

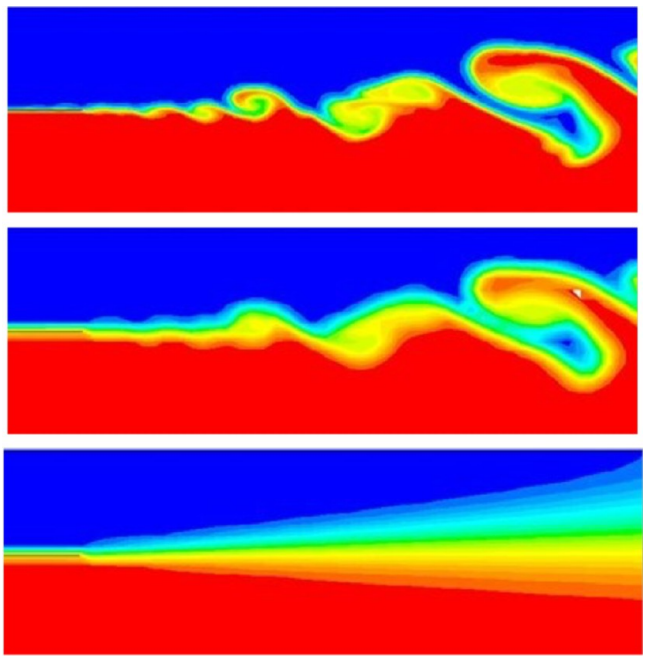

Figure 3. Levels of spatial resolution attained in flow simulations using DNS (top), SRS (middle), and RANS (bottom) approaches. Reproduced with permission from ref 76. Copyright 2011 ANSYS, Inc.

Direct Numerical Simulation (DNS). DNS numerically solves the full, unsteady Navier–Stokes equations without using any simplified turbulence models. For accurate predictions, the time scales and length scales need to be well-resolved. For length scales, the lower limit of mesh size required for simulations is defined by the Kolmogorov microscales, the smallest length scales at which turbulence dissipation takes place. Similarly, the step for time marching must be chosen such that the fluid element moves a fraction of the smallest length scale. Both the mesh size and the number of time steps required for DNS turbulence modeling are proportional to the Reynolds number (Re) and hence become computationally expensive under the conditions of interest in melt blowing. Typically, melt blowing simulations using DNS require time steps on the order of 10^{-10} s and small grid sizing on the order of 10^{-6} m.

Scale Resolving Simulation (SRS). In SRS, the largest eddy currents are calculated in a domain that helps in understanding the behavior of large swirling flows, visualizing flow separation, studying acoustics, and investigating systems that are particularly sensitive to turbulent behavior. SRS helps resolve a larger spectrum of turbulence as compared to Reynolds-Averaged Navier–Stokes (RANS) modeling (described later). Due to the need for relatively inexpensive computational resources, the SRS model is often employed in free-stream simulations as the no-slip boundary conditions applied to surfaces require finer meshing to obtain more realistic results.

Within the SRS regime, the Large Eddy Simulation (LES) is proposed to be superior to k-ϵ and other variants of RANS models. In LES, the large-scale motions of turbulent flow are computed directly, while simplified models are used for the small-scale motions. Small-scale motions represent those at subgrid lengths. This approach results in a significant reduction in computational cost compared to DNS. LES is more accurate

https://doi.org/10.1021/acs.iecr.1c03444
Ind. Eng. Chem. Res. 2022, 61, 65–85

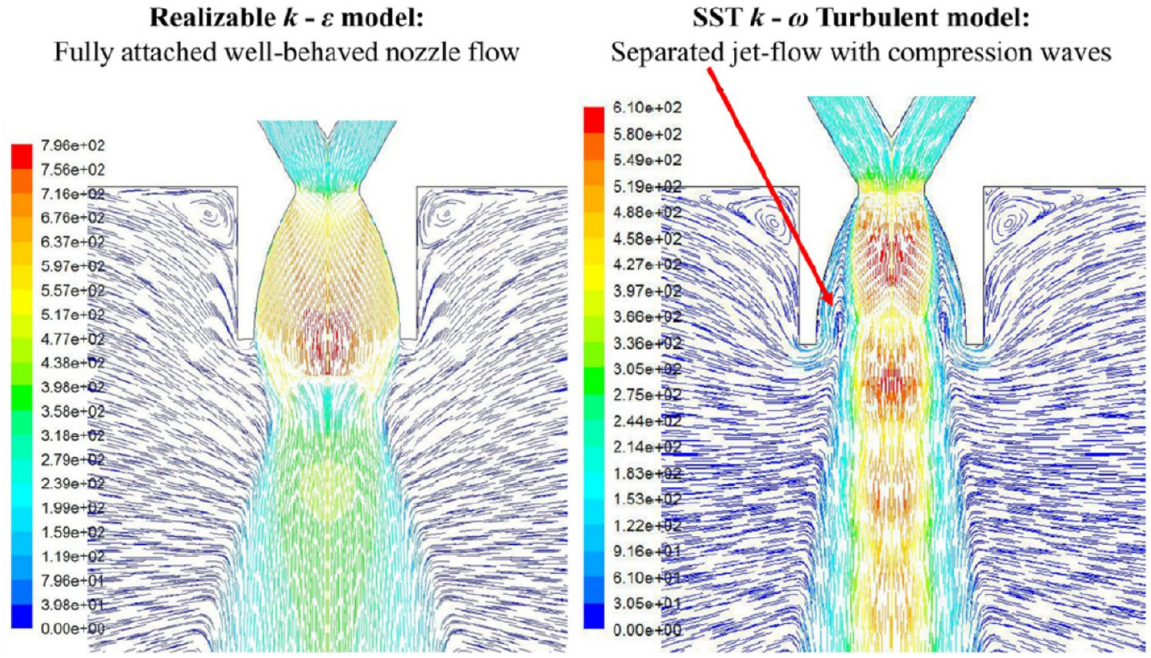

Figure 4. Comparing two turbulence models for nozzles after die exit. Colored streamlines represent velocity field in units of (m/s). Reproduced with permission from ref 12. Copyright 2012 Elsevier.

than the RANS approach since LES captures large eddies in detail; large eddies carry most of the turbulence energy and are responsible for turbulent mixing.

The small-scale eddies, which tend to be more isotropic and homogeneous than the large ones, are modeled separately compared to RANS, which models all scales using a single model. Therefore, LES is a more viable and promising numerical tool for simulating realistic turbulent or transitional flows. LES is less dissipative and can discern changes in the flow field for time steps as small as 0.1 μs.[2] Specifically, LES proves useful in understanding the fiber whipping motion which is attributed to the large turbulence eddies formed by the interaction between hot and ambient air.[6]

Reynolds-Averaged Navier−Stokes (RANS). The RANS technique employs methods to smooth out severely turbulent behavior and is often used to get the steady-state operation of fluid flow. RANS employs the idea of decomposing the flow variable, e.g., the instantaneous velocity (u) into a time-averaged component ($\overline{u}$) plus a fluctuating component (u'), where the time-average of the fluctuating component vanishes. The procedure involves substituting this expression for velocity into the linear momentum balance in Navier−Stokes equations and taking a time-average to eliminate the fluctuating term. Although RANS accurately predicts the mean flow variables in most cases, it often fails in cases of complex flows in melt blowing such as unsteady flow features dominating the flow field. However, it is the computationally least expensive in modeling melt blowing processes and closely captures most of the flow variables. Hence, it is the most widely used technique in the field.

For an incompressible Newtonian fluid having density ρ and viscosity μ, the RANS equation for linear momentum takes the following form (in Einstein notation)

$$\rho\overline{u_j}\frac{\partial\overline{u_i}}{\partial x_j} = \rho\overline{f_i} + \frac{\partial}{\partial x_j}\left[-\overline{p}\,\delta_{ij} + \mu\left(\frac{\partial\overline{u_i}}{\partial x_j} + \frac{\partial\overline{u_j}}{\partial x_i}\right) - \rho\overline{u_i'u_j'}\right] \quad (1)$$

where $\overline{f_i}$ denotes a mean body force, and the first, second, and third terms in the square bracket represent the isotropic stress due to pressure, the viscous stresses, and the 'Reynolds stress' due to the fluctuating velocity components.

The Reynolds stress term in eq 1 remains an unknown quantity, and hence we require additional equations, referred to as 'closure equations', to eliminate any reference to the fluctuating unknown velocity components in modeling the turbulence (discussed below). RANS requires significantly less computational resources than SRS and DNS. It contains various models used for fluid simulations near walls, in freestreams, and for extreme operating parameters that cannot be tested with conventional instrumentation.

RANS is coupled with simplified models like the Reynolds Stress Model (RSM), the k-ϵ model, and the k-ω model. In the k-ϵ and k-ω models, the Reynolds stresses are expressed in terms of the eddy-viscosity, μ_t ($\mu_t = \rho C_\mu k^2/\epsilon$; C_μ being a known constant), and require additional equations governing transport of turbulent kinetic energy (k) and turbulent energy dissipation (ϵ). RSM directly computes the values of different components of Reynolds stresses using the general transport equation in the formulation. RSM is the most complete classical turbulence model that retains good accuracy of fluid simulations and has been used extensively to study air flow fields in the melt blowing process.[21,23] For example, RSM models appear to reproduce a blunt-die system better than alternative RSM models, such as the standard and realizable k-ϵ.[24,25]

The k-ϵ model solves a coupled set of partial differential equations governing the evolution of turbulent kinetic energy (k) and dissipation of kinetic energy (ϵ). It is particularly

https://doi.org/10.1021/acs.iecr.1c03444
Ind. Eng. Chem. Res. 2022, 61, 65−85

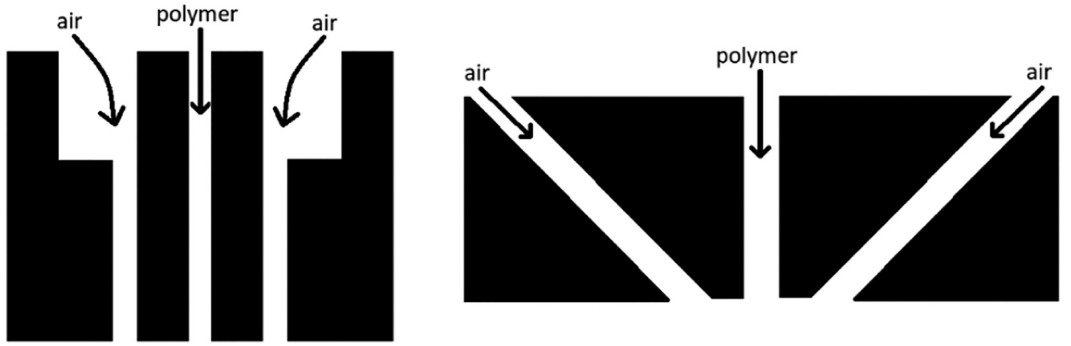

Figure 5. Schematic of the annular die (left) and slot die (right).

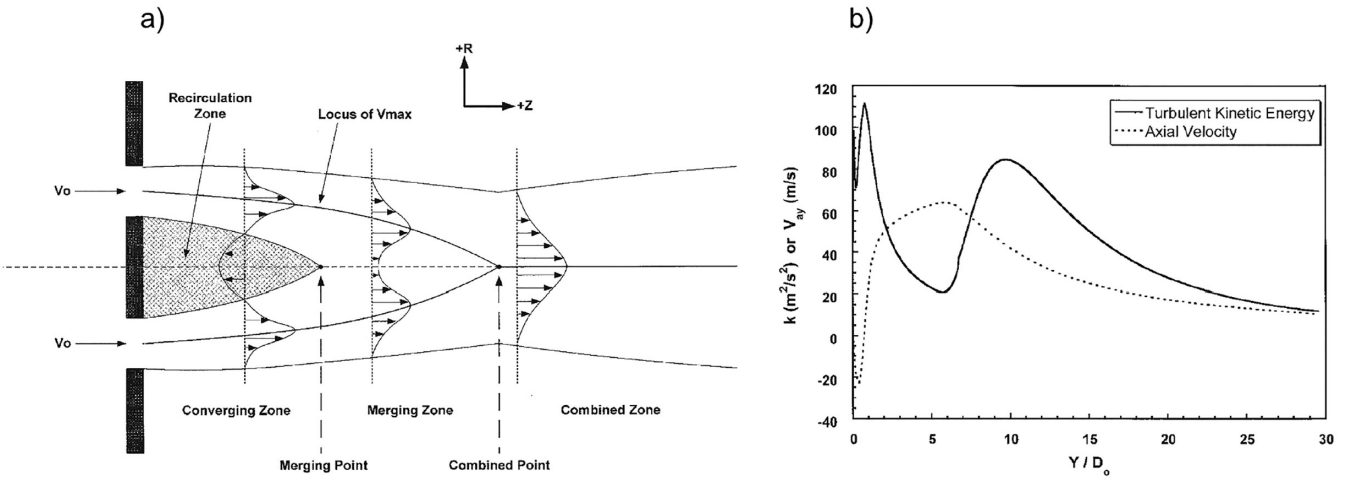

Figure 6. a) Diagram of the different zones of air flow field development for an annular jet by Lai et al.[37] b) Model predictions of centerline axial velocity and turbulent kinetic energy by Moore et al. using CFD simulations. Reproduced with permission from ref 32. Copyright 2004 John Wiley and Sons.

useful for systems involving high Reynolds number.[26,27] The governing equations in this model are as follows

$$\frac{\partial(\rho k)}{\partial t} + \frac{\partial(\rho k u_i)}{\partial x_i} = \frac{\partial}{\partial x_j}\left[\frac{\mu_t}{\sigma_k}\frac{\partial k}{\partial x_j}\right] + 2\mu_t E_{ij}E_{ij} - \rho\epsilon \quad (2)$$

$$\frac{\partial(\rho\epsilon)}{\partial t} + \frac{\partial(\rho\epsilon u_i)}{\partial x_i} = \frac{\partial}{\partial x_j}\left[\frac{\mu_t}{\sigma_\epsilon}\frac{\partial \epsilon}{\partial x_j}\right] + C_{1\epsilon}\frac{\epsilon}{k}2\mu_t E_{ij}E_{ij} - \rho C_{2\epsilon}\frac{\epsilon^2}{k} \quad (3)$$

where $C_{1\epsilon}$, $C_{2\epsilon}$, σ_ϵ, and σ_k are known constants.

However, the constants used in this model must usually be adjusted, manually or through an algorithm, to account for turbulence both near and far from the die.[26,28] This model qualitatively agrees with experiments in predicting fluid behavior in a free stream. There exist other variants of the k-ϵ model such as the standard k-ϵ and realizable k-ϵ. However, for large airstream strain rates typically found in the melt blowing process, the standard k-ϵ may not yield realistic results.[25]

The k-ω model is similar to the k-ϵ model but specializes in calculating turbulence near the surfaces where the no-slip boundary condition is present. The Shear-Stress-Transport (SST) k-ω model (a variant of k-ω) combines the near-wall competence of the k-ω model and the far-wall competence of the k-ϵ model.[23,24] Hassan et al. compared the SST k-ω model against other models such as the k-ϵ, realizable k-ϵ, and RSM and found it to be more suitable for rocket nozzle simulation where the fluid detaches from the nozzle wall as observed in experimental studies.[24] A similar comparison between the realizable k-ϵ and SST k-ω turbulence models is shown in Figure 4.

Optimizing Air Flow with Die Geometry. In the melt blowing process, the initial region after the fiber exits the die is critical since the high-temperature air attenuates the fiber by a factor of around 250 within microseconds.[28−30] Higher temperatures along the centerline of the die lead to finer fibers as the complete polymer solidification is delayed. Therefore, maintaining such high temperatures axially and minimizing temperature decay close to the die are crucial for fine fiber formation.[19,31]

Maximizing air−fiber friction is another key aspect in the formation of finer fibers. Decreasing the polymer feed rate at constant airspeeds leads to finer fibers due to a higher relative velocity and thus an increase in the drag force. However, decreasing the polymer feed rate restricts higher fiber yields that are desirable in large-scale manufacturing.[19,28] Thus, the restriction on the feed rate and the coupling of the temperature decay to the air flow profile plays a critical role in fiber formation.

Several die geometries have been implemented in the melt blowing process and serve as a common topic of interest. Each die geometry gives rise to different air flow profiles that must be analyzed to produce minimal turbulence and maximize airspeed and temperature retention. Some common die

https://doi.org/10.1021/acs.iecr.1c03444
Ind. Eng. Chem. Res. 2022, 61, 65−85

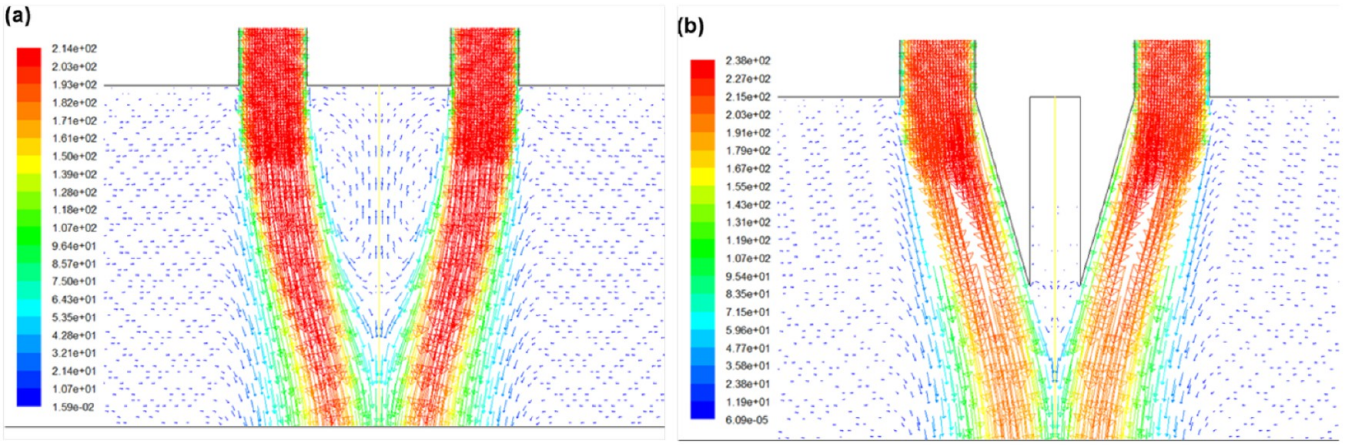

Figure 7. Eddy currents in a recirculation zone (region between the two jet streams near the die exit) a) with and b) without "wing" protrusions. Colored scale is given in units of (m/s). Reproduced with permission from ref 19. Copyright 2013 American Chemical Society.

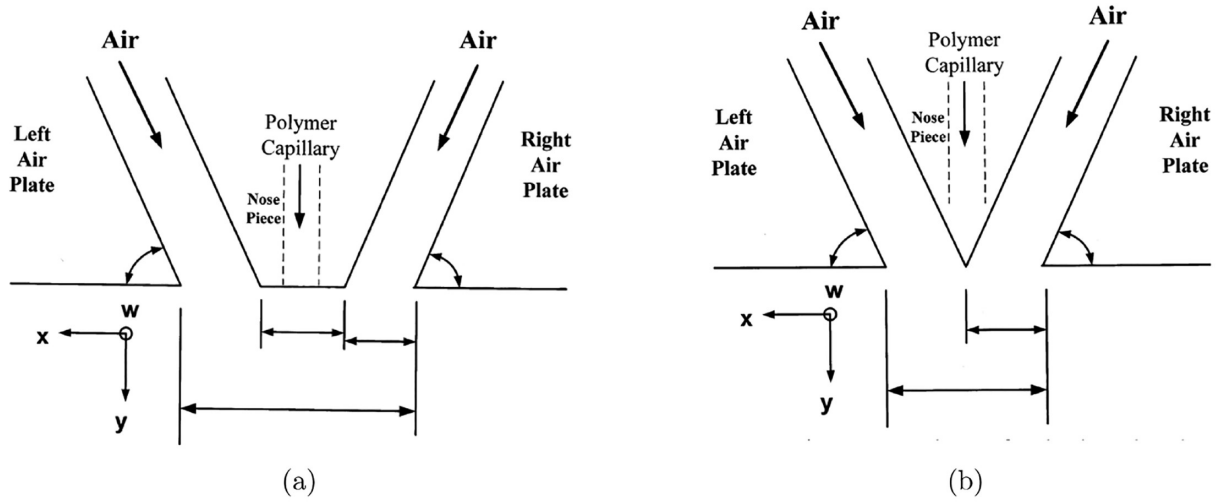

Figure 8. Schematic of (a) flush blunt and (b) flush sharp slot dies. Reproduced with permission from ref 18. Copyright 2004 American Chemical Society.

geometries include annular, slot, and modified slot. Annular die and slot die geometries are shown in Figure 5.

Annular Dies. In the case of annular dies, the air and polymer streams are parallel, and the air flow encircles the polymer stream. Moore et al. modeled the air flow field of an isothermal annular jet using the FLUENT toolbox[32] and compared the model predictions to earlier experimental measurements.[33,34] The presence of fiber in the jet stream was neglected. Apart from studying the centerline velocity, the mean velocity spreading rate was also studied, an important aspect of modeling turbulent jets. The velocity spreading rate depends on the turbulent transport of momentum away from the jet and the mass transport from stationary air into the jet stream.

RSM (see Launder et al.[35]) was chosen by Moore et al. to model turbulence; the equation for the transport of Reynolds stresses was given by Durbin et al.[36] The model captures the three zones of the air flow field development from the die exit (converging zone, merging zone, and well-developed region) reasonably well, including the negative centerline velocity in the converging zone as shown in Figure 6.[32] The simulation results agree well with experimental data (specifically, the velocity magnitude, velocity decay rate, and velocity spread rate) and provide a useful tool for designing annular jet orifices.

The measurement of turbulence quantities, more commonly the turbulent kinetic energy associated with turbulent velocity fluctuations, is also of importance to the melt blowing process. Strong velocity fluctuations can lead to fiber sticking to the die face or fiber entanglement with itself or with adjacent fibers. Although the experimental measurement of turbulence quantities can be difficult, simulations can provide information on the state of turbulence within the flow.

On comparing predictions of turbulent kinetic energy with different air flow rates, it was observed that at higher air flow rates, the effects of air compressibility become significant.[32] Such effects were prominent closer to the die than at large distances from it. Thus, to study the melt blowing process with high nominal velocities (velocities > 100 m/s) more accurately, the compressibility of air needs to be taken into account for the calculation of the air flow field close to the die. Moreover, the simulations suggest that the air flow field of an annular jet has significant turbulence anisotropy, larger Reynolds stresses along the axial direction than any other direction. This may potentially explain why the RSM model performs better than the simpler yet popular k-ϵ or k-ω models

https://doi.org/10.1021/acs.iecr.1c03444
Ind. Eng. Chem. Res. 2022, 61, 65−85

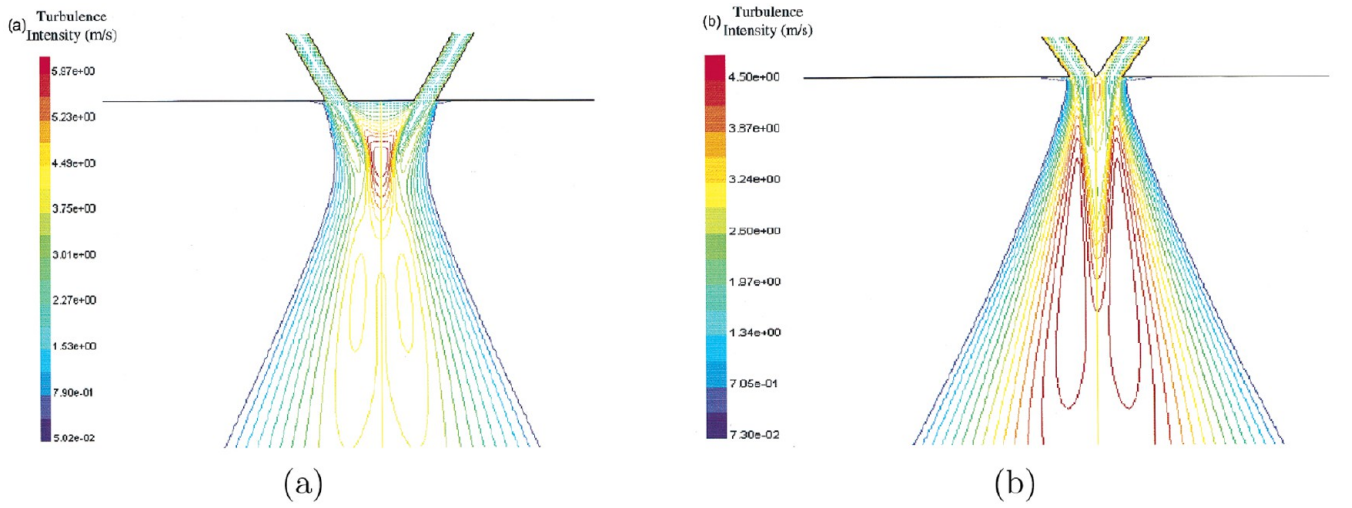

Figure 9. Turbulence intensity in the blunt die (a) and sharp die (b) with units of turbulence intensity given in (m/s). Reproduced with permission from ref 25. Copyright 2002 American Chemical Society.

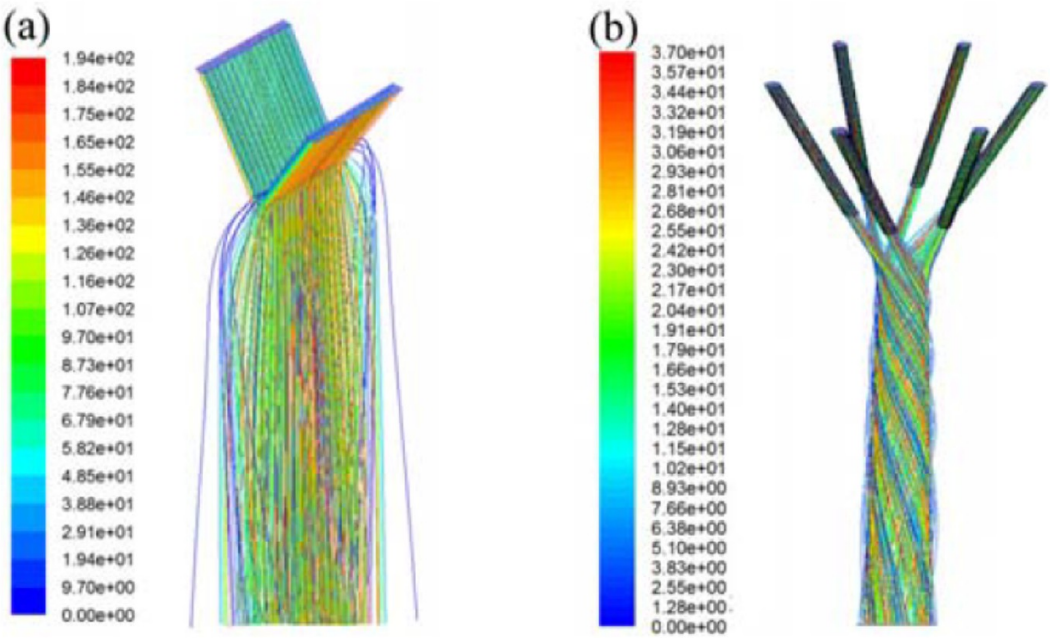

Figure 10. 3D CFD air flow field simulations of (a) slot dies and (b) spiral dies. Streamlines indicate velocity magnitude given in units of (m/s). Reproduced with permisssion from ref 39. Copyright 2017 The Authors under Creative Commons CC-BY 3.0, published by IOP Publishing.

in describing turbulent melt blowing jets. The latter models make the assumption of turbulence isotropy.

Wu et al. studied the air flow field in a melt blowing process with an annular die geometry for nonisothermal conditions.[28] The air velocity profiles were found to be similar to those described by Moore et al.[32] As for the air temperature profile, there is a region of high air temperature just near the die, which is in favor of the polymer drawing; a maximum temperature is attained very close to the annular die exit. The air temperature decreases along the axial direction similar to the air velocity.

In regions close to the die exit, a recirculation zone appears between the two jet streams, where eddy currents deter fiber attenuation as the air velocity is opposite to the velocity of the fiber along the centerline as seen in Figure 7a. Wang et al. utilized protruding "wings" that interrupt the air flow circulation (shown in Figure 7b), thus suppressing the formation of eddies which interrupt air flow and disperse thermal energy.[19] These protrusions also serve to mitigate fiber breakage as the fiber does not bend and twist to an extent that it would in the presence of turbulence close to the die exit. CFD simulations show that the winged protrusions decrease eddy currents, increase centerline air velocity, and minimize air fluctuations and thermal decay over significant distances from the die.[19] In general, the annular die geometry proves favorable in fiber drawing as the air and polymer streams are nearly parallel and the air flow encircles the polymer stream.[28]

Slot Dies. In slot dies, converging air jets exit at an angle, meeting in front of the die to attenuate the fiber (shown in Figure 8 for two different variations of slot die geometries). This die variant has the advantage that the air meets the polymer fiber at relatively higher speeds near the die exit as

https://doi.org/10.1021/acs.iecr.1c03444
Ind. Eng. Chem. Res. 2022, 61, 65−85

compared to the annular die. However, the colliding air streams also cause excessive turbulence which may lead to defects, where fibers stick to the die face or other surrounding fibers.[25,38]

Simulations, using RSM to model turbulence, reveal that a recirculation zone appears near the die exit, similar to one previously described for annular dies, that can hinder fiber attenuation.[25] This turbulent region often leads to fiber whipping and breakage near the die.[9] Although the authors could quantitatively predict the experimental mean air flow quantities by manually adjusting the model constants, the turbulence characteristics, including the recirculation zone properties, could not be verified due to experimental constraints in measuring the quantities of interest close to the die exit.[25]

Krutka et al. showed that for larger die angles (air channels approaching parallel to polymer stream) the maximum turbulence occurs further from the die and is lower in intensity than smaller angles. A possible explanation is that air streams lose energy to ambient air before meeting each other at a point further from the die exit.

Among the blunt and sharp slot die geometries, it was found that the blunt die produces less turbulence at the die exit compared to the sharp die. The latter produces two turbulent regions, one near the tip and another further away but yields higher air velocities (shown in Figure 9).[25] The blunt die exhibits a turbulent spot at a smaller distance away from the die that quickly dies out. A trade-off exists between stability and velocity for the different die geometries both of which may be useful depending on the operating conditions. It is observed that large differences in the maximum and minimum airfield velocities result in large deviations in fiber quality.[38]

Xie et al. simulated slot dies and other variants (like spiral dies) in 3D and compared their fiber photography results. It was concluded that the fiber path was highly dependent on the air flow field, larger velocity spread in the transverse direction for the conventional slot die as compared to an isotropic spread for spiral die as shown in Figure 10.[39] This observation is useful in forming various types of fiber webs by tuning the air flow fields using different die types and geometries.

Marla et al. performed nonisothermal simulations and found that within 1 cm of the slot die nosepiece, the fiber temperature suddenly increases due to the high air temperature and lack of ambient air cooling and decays eventually further downstream.[18] Xie et al. studied the temperature fluctuations in the air flow field and found them to be much more regular than the fluctuations in air velocity, as they conformed to a bimodal distribution with a stable repetitive frequency.[38] These temperature fluctuations cause changes in the air flow field further from the die. However, excessive temperatures, although conducive to postpone the fiber solidification process, can lead to energy losses and fiber rebounding (fiber reheating and increasing in diameter). Hence, understanding how the temperature distribution affects the air flow field and fiber integrity simultaneously is important.

Different modifications of the slot die geometry are studied with regards to the air flow field velocity distributions and turbulent fluctuations. A useful variation of the blunt- and sharp-tip dies is to move the nosepiece either inward (inset type; shown in Figure 11) or outward (outset type) from the die face to modify the airfield. CFD simulations reveal that inset dies (both sharp and blunt) lead to higher centerline velocities but also increased turbulence when compared to

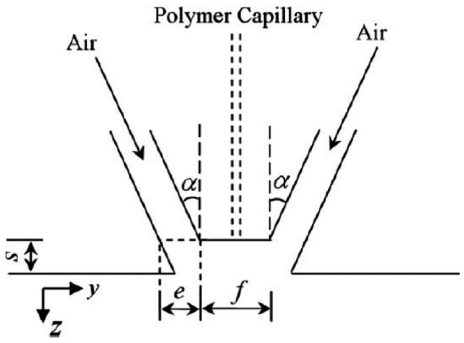

Figure 11. Inset blunt die geometrical parameters. Reproduced with permission from ref 21. Copyright 2011 John Wiley and Sons.

flush dies.[20,26] However, the inset configurations may cause blockage in the die when fibers stick to the air plates on either side of the nosepiece.[26] An outset die reduces turbulence fluctuations at the die tip leading to less fiber breakage. However, a drawback of the outset die geometry is that it has lower centerline speeds as compared to the inset die.[20,40]

An early goal of any simulation is to evaluate its ability to reproduce key experimental results to build credibility in the model before it is used to predict the behavior for other configurations/process parameters. The optimal die geometry cannot always be calculated as the melt blowing process has several factors that are coupled. This usually means new advancements are partly driven by intuition and trial-and-error testing.

Sun et al. adopted the approach of using a multiobjective optimization using a genetic algorithm (MOGA) framework with a vector-evaluated genetic algorithm (VEGA), to test various die geometries to optimize the air flow field with the lowest velocity and temperature decay for melt blowing using a slot die.[21] This method relies on randomly sorted populations, later split into two subpopulations, to maximize the desired function via mutations until the best "offspring" is produced. This method can, therefore, modulate several parameters for die geometry and produce a sample set of the geometries that maximize air velocities and temperatures. While this method is not the only way to optimize the melt blowing process, it manages to give a holistic picture of various factors affecting the melt blowing process performance.

Sun et al. tested 1000 different slot dies using MOGA to find the optimal air flow field within the range of values tested for various geometric parameters as shown in Figure 11 and found that a blunt nose die of width 2.015 mm (f), slot width 1.988 mm (e), inset 1.393 mm (s), and an angle of 11.19° (α, with respect to the vertical axis) yielded the optimum processing conditions, with the lowest velocity decay and temperature decay.[21] Chen et al. found qualitatively similar results and concluded that inset dies with an inset distance of 0.75 mm yields fibers 34.1% finer than flush dies.[26] Simulations by Sun et al. show that smaller angles (with respect to the vertical plane) and larger slot widths minimize decay in air velocities and temperature.[21] This reveals that an optimal die geometry lies closer to an annular die with a slight angle offset and an inset nosepiece.

It can be difficult to assess comparative air flow field performance under various die geometries. Krutka et al. sought to rectify a portion of this issue by using a self-similar solution with varying parameters to describe the centerline velocity for

https://doi.org/10.1021/acs.iecr.1c03444
Ind. Eng. Chem. Res. 2022, 61, 65−85

various inset, flush, and outset sharp and blunt dies with the following[40]

$$\frac{\left(\frac{V_o}{V_{jo}}\right)}{\left(\frac{V_o}{V_{jo}}\right)_{z=z_{max}}} = e \times \left(\frac{z}{z_{max}}\right)^{-f} \quad (4)$$

where f and e are dimensionless constants used for curve-fitting different die geometries, z_{max} is the distance from the die exit where the centerline velocity reaches a maximum value, V_o is the maximum velocity of the jet, V_{jo} is the nominal discharge velocity defined as $V_{jo} = (1000{*}Q)/(2b_o l)$, l is the length of air slots in the y-direction, b_o is the face width of the die slot, and Q is the air flow rate through both slots. Different die geometries appeared to fit this curve well, allowing for estimation of the centerline velocity, its location, and the maximum turbulence intensity without running a full CFD simulation.

Schwarz Die. The Schwarz die is designed to produce several fibers simultaneously by using an array of annular dies as shown in Figure 12.[41] The array-like structure of orifices in this die introduces several additional complexities, such as the effect of distance between the jets on fiber quality, temperature, and air velocity decay, due to interference with the adjacent dies. One such observed effect is that increasing the jet diameter leads to higher temperatures close to the die.[41]

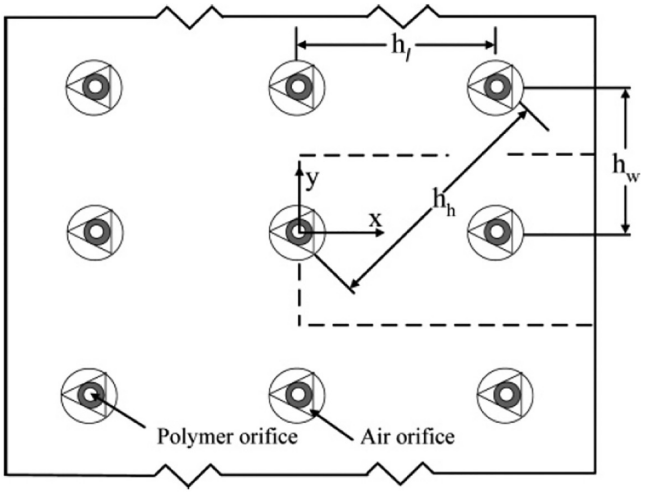

Figure 12. Schwarz die front view. Reproduced with permission from ref 41. Copyright 2006 American Chemical Society.

Having several jets in proximity in the same simulation domain as opposed to a single, isolated jet will introduce additional complexities in the air turbulence and polymer fiber modeling. Krutka et al. used the ideal gas equation to accurately model the compressibility of air and the effect of fibers in the air flow field.[30] They also found that the RSM model failed to converge for 3D air flow modeling and resorted to a simpler k-ϵ model to match experimental results further from the die.[1] However, with the presence of a fiber disrupting the airfield, the RSM model was used to study the air flow close to the fiber.[30]

Observing the air flow field in a multijet arrangement shows that there is a self-similar structure in the air flow field, with recirculation and merging zones present where different air streams interact (shown in Figure 13).[1] Moving further from the die, the distinct air jets begin to merge as they exchange energy with each other and the ambient air, increasing the spacing between jets helps delay this merging.[1] The outer jet streams are usually pulled toward the inner jet streams because they experience a biased frictional force with the ambient air on the outside forcing the air streams to follow nonlinear trajectories. This suggests the possibility of an optimal die spacing to yield air velocities that produce finer fibers that are defect-free without expending much additional energy. A deeper fundamental understanding of the turbulence interactions between multiple jets in Schwarz dies might be obtained using the LES technique to capture time-dependent turbulence quantities.[41]

Augmenting Air Flow after the Die Exit. In the melt blowing process, several modifications can be added after the die exit to minimize the turbulence fluctuations and promote uniform fiber formation. Turbulence in air flow can lead to fiber whipping or fiber entanglements causing uneven fiber formation, breakage of fibers, and complications in fiber laydown onto the web. CFD simulations help understand the air flow field when modifications are made after the die exit to control the air flow.

Constrictors. A constrictor is a barrier introduced after the exit to help minimize turbulence and control the temperature profile. Hassan et al. simulated constrictors of different lengths, angles, and lateral distances from the die exit to understand their effect on the air flow field. It was found that constrictor angles of 45 and 60 degrees (from horizontal plane) maintain the desired centerline air velocity and temperature without introducing significant turbulence.[24] Constrictor widths of 20−30 mm maintain the desired centerline air velocity and temperature by accelerating the air flow and increasing the drag force necessary to attenuate or stretch the fiber to smaller diameters.[24,42] However, lateral widths of less than 10 mm cause eddy currents to form close to the centerline (Figure 14) which lead to fiber whipping and entanglement at early times.[24,42] These simulation results were verified using complementary experiments.

Interestingly, constrictors of 14 mm width produced fibers that were 20−40% smaller in diameter than those without constrictors. Moreover, constrictor lengths between 10 and 20 mm proved optimal to minimize temperature decay.[24] The advantage of using longer constrictors is that higher temperatures are attained near the die exit. However, constrictor lengths greater than 20 mm lead to turbulence and may cause fibers to stick to the constrictor walls.

Chelikani et al. performed simulations to test the 'Coanda effect', when fluid streams stick to convex surfaces, using flat and curved walls, which can be used to enhance the production of fine fibers. Using nondimensionalized distances (dividing distance by the simulation length scale, i.e., x/L_x) they found that flat walls should be 0.25 units away (shown in Figure 15) and curved constrictors should be 0.5 units away from the nozzle to maximize the Coanda effect.[43] Chelikani et al. show that a flat wall of 7.5 mm width and 35 mm length gives the most suitable process conditions, contrary to the results by Hassan et al.[24] The differences could be attributed to the angle of the slot dies or the different turbulence models used (3D RANS by Chelikani et al. vs the k-ϵ model by Hassan et al.).

Nozzles. A central idea for improving the melt blowing process performance is to promote fiber attenuation through higher air velocities and minimize fiber whipping and

https://doi.org/10.1021/acs.iecr.1c03444
Ind. Eng. Chem. Res. 2022, 61, 65−85

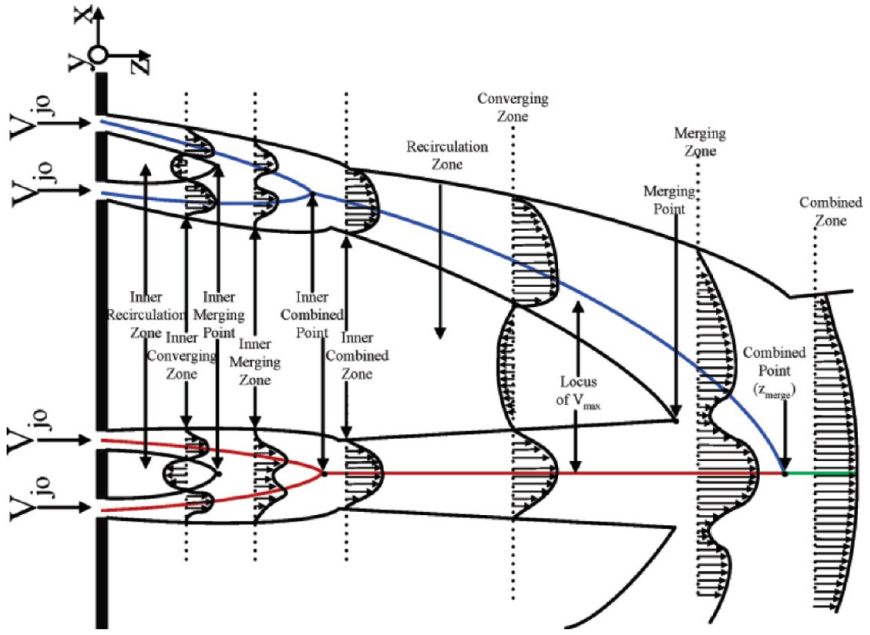

Figure 13. Different zones of air flow field development for a Schwarz die. Reproduced with permission from ref 1. Copyright 2005 American Chemical Society.

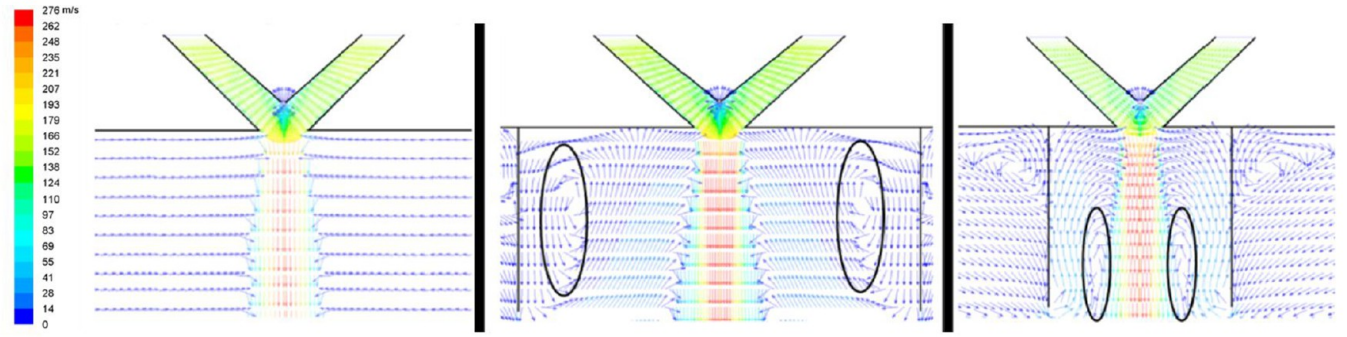

Figure 14. Effect of constrictor widths on the formation of eddies. Colored vectors are velocity magnitude ranging from 0 to 276 m/s. Reproduced with permission from ref 24. Copyright 2016 American Chemical Society.

entanglement by reducing turbulence. Tan et al. attempted to address this by introducing a converging-diverging Laval nozzle (a convergent-divergent nozzle, producing supersonic flows in the divergent section and choked flow conditions at the narrowest point) after the die exit to enhance airspeeds in a controlled manner.[12] A major challenge in using nozzles is the formation of compression waves that leads to air instabilities and improper fiber formation. However, by carefully controlling the inlet pressure, compression waves could be moved further back into the nozzle leading to fewer instabilities and less fiber whipping (shown in Figure 16).[12] Another challenge in using nozzles is the requirement to operate the process above the speed of sound; this is difficult to maintain and may lead to in-plant operational challenges.[24] Despite these challenges, two different nozzle designs were able to achieve peak speeds of Mach 2.3 and Mach 3 outside the die, with close agreement to experimental measurements.

Verifying Model Predictions with Experiments. It is important to complement simulation results with experiments to ensure that the model predictions make physical sense. However, experimentally characterizing the air flow requires the introduction of an instrument into the airfield which interrupts air flow and can lead to fibers sticking to the instrument.[29] Despite the challenges involved, several methods have been used to measure the air velocity and temperature fields in the melt blowing process.

Some of the earlier studies involved the use of pitot tubes for measuring air velocities and thermocouples for measuring air temperatures.[44−46] However, measurements using pitot tubes and thermocouples give only the mean velocity and mean temperature of the airflow field, while often not capturing fluctuations in these variables. Understanding these fluctuations is critical to the study of air flow turbulence and fiber whipping motion. Moreover, pitot tubes perform well in low-velocity flow fields.

The use of Laser Doppler Velocimetry (LDV), a non-intrusive method using light to measure particle velocities in the flow field, and hot wire anemometry allow for obtaining one, two, or three components of the air velocity in melt blowing but are limited to regions far from the die.[25] These techniques can measure higher values of air velocity. The hot wire anemometer helps measure the instantaneous velocity at any point in the air flow field, which can be related to the turbulence fluctuations in the air stream.[47] Further innovation

https://doi.org/10.1021/acs.iecr.1c03444
Ind. Eng. Chem. Res. 2022, 61, 65−85

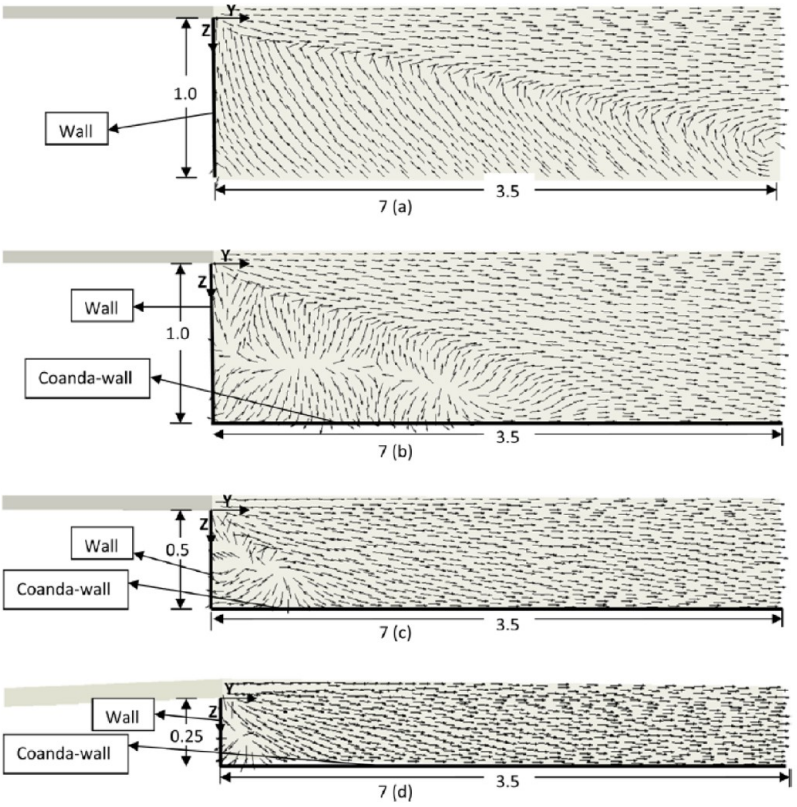

Figure 15. Comparing air flow fields (velocity vectors) with a constrictor at different distances. Reproduced with permission from ref 43. Copyright 2013 American Chemical Society.

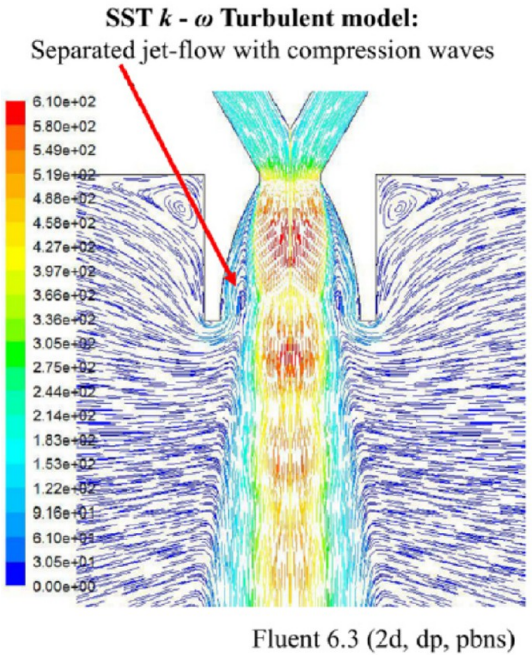

Figure 16. Air flow field simulation using a laval nozzle. Colored streamlines represent velocity field in units of (m/s). Reproduced with permission from ref 12. Copyright 2012 Elsevier.

by Xie et al. into advancing experimental techniques to probe turbulent air flows included a hot-wire anemometer with a two-dimensional velocity probe (two wires placed in parallel planes with perpendicular projections).[38] The authors also used a single wire probe to separately measure air temperature fluctuations to help analyze coupling between air temperature and velocity.[38]

Yang and Zeng carried out simultaneous real-time measurements of temperature and velocity fields for the first time using an X-wire hot wire anemometer.[48] Their experimental setup helped analyze the thermal and turbulence characteristics of the air flow field and correlation between the two in a nonisothermal melt blowing process. When studying lateral air flow especially in the turbulent regime, LDV proves very useful.[18] Imaging the air density with Schlieren visualization is useful in studying nozzles after the die exit as it can capture images of compression waves that cause excessive turbulence in the airfield.[12]

Another technique called the particle image velocimetry (PIV) is used to measure the turbulent air flow field in the melt blowing process in an effort to explain the fiber whipping motion.[49] The PIV technique involves emitting numerous tracer particles into the air flow field and then using a pulsed laser beam to detect their trajectory. PIV helps visualize the structure of the turbulent air flow and measure the spatial distribution of the velocity at any time instance. These quantities are difficult to obtain using a pitot tube, hot-wire anemometer or LDV. Moreover, PIV helps study the time evolution process of turbulent air flow which can be combined with fiber path imaging to develop deeper insight into fiber whipping dynamics. In most studies to date, high-speed photography has been employed to capture the fiber motion between the die and collector.

Fiber Simulations. Melt blowing involves extruding a molten polymer through a die orifice where jets of hot air create frictional drag forces on surfaces, drawing the fiber and reducing its diameter.[50] The fiber experiences internal and

https://doi.org/10.1021/acs.iecr.1c03444
Ind. Eng. Chem. Res. 2022, 61, 65−85

external heat transfer and internal friction and fluid forces during the process. While these factors introduce complexities in modeling the fiber dynamics, well-placed assumptions can simplify the model to enable understanding of final fiber characteristics.

A more robust melt blowing model is built by coupling fiber simulations in 3D to CFD simulations of air flow to simulate fiber whipping and other complex phenomena.[51] As discussed previously, modeling the air dynamics often hinges on the assumption of neglecting the presence of fiber in the complex airfield. However, in the modeling of fiber dynamics, the presence of the surrounding air jet is often incorporated through a term for drag force of the air at the fiber boundary.[2,23]

It is also necessary to have a suitable boundary condition at the whipping end (axial end) of the fiber. One technique often used is to label a 'stop point' where the stress in the fiber vanishes or where the fiber velocity matches the air velocity around it.[50] To compute the stop point, an initial guess is made for the stress at the beginning of the fiber and propagated down to a point where the stress vanishes.[50] Some models used to study fiber dynamics are presented in this section.

DIFFERENT FIBER SIMULATION TECHNIQUES

Fiber Models. Fibers can be represented as beads of masses connected by springs along one dimension as shown in Figure 17, which help simulate internal forces within the polymer fiber.[23] The springs represent the elasticity of the fiber while the bending deflection in successive springs coincides with the fiber flexibility. The mass element "bead" can be designated as the center of the fiber and simplifies the tracking of other elements. This helps in postprocessing the movement of the fiber during the melt blowing process.[22] However, a challenge in using this technique is that the lower free end of the fiber acts as a varying boundary condition which can be difficult to incorporate.[22,50] For small pieces of a broken fiber, the internal restoring force is minuscule compared to the external drag force, and assumptions of constant fiber diameter and invariant length can be made.[23]

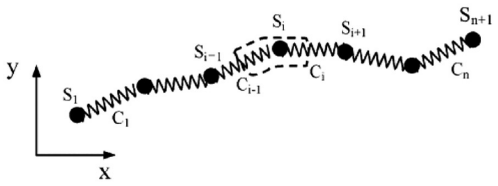

Figure 17. Schematic of short fiber fragment. Reproduced with permission from ref 23. Copyright 2005 American Chemical Society.

A more complete 3D model of the fiber requires fewer assumptions and relies on equations of continuity, momentum, and energy for internal heat transfer.[22] While not all models consider heat transfer as a core element, continuity and momentum must be computed if the fiber motion is to approach a realistic representation. A good check for complex fiber motion is to ensure that the 3D model predictions can collapse onto 2D and 1D fiber models and can be further validated with fiber amplitude, frequency, and other motion-related phenomena that cameras can record in experiments.[22,52]

Fiber models can also be as simple as the viscoelastic element-bead model to include some damping elements that help reflect energy loss mechanisms due to viscoelastic forces within the fiber. In essence, these models mimic elements found in Maxwell and Kelvin−Voigt's spring-dashpot models. Han et al. used several different models constructed from spring, mass, and damping elements (such as those shown in Figure 18) and concluded that the SLS model predicts fiber characteristics (diameter, velocity, and stress) more accurately than other comparable models.[53]

Fiber Web. Another key aspect of fiber simulations is understanding the fiber collection process and assessing the quality and characteristics of the final fiber web. Ghosal et al. studied this aspect and developed a fiber model dependent on touchdown times to calculate the 3D structure of the fiber web to determine properties such as porosity, thickness, structure, permeability, and other nonwoven properties (shown schematically in Figure 19).[8] At the fiber collection end, where the fiber contacts the collector plate, Ghosal et al. demonstrated that increasing the collector plate speed tends to increase the nonwoven porosity and permeability due to fewer fiber layers being placed down in a given area. Yarin et al. constructed a similar model that could predict fiber deposition patterns and their distribution.[11] These techniques can be useful in selecting the optimum collector speed to obtain desired fiber qualities. Yarin et al. showed that the turbulence in air flow and collector speed do not correlate to mean fiber diameter.[11] It was also predicted that the fiber diameter distribution approaches a normal distribution with an increase in the collector screen velocity.

Failure Methods in Fiber Formation. Some common fiber defects caused by the air flow field that occur in the melt blowing process are flies (broken fibers), shots (polymer particles embedded in the fiber mat), and jams (adhesion between fiber segments).[6,9] A typical fiber breakage in the air flow is shown schematically in Figure 20. Rayleigh instabilities are a potential source of fibers becoming unstable and breaking into small droplets, thus imposing a limit on how thin the fibers can become.[54] Simulations are used to get deeper insights into the formation of such fiber defects and minimize their occurrence.

Most fiber simulations assume a continuous filament model that does not account for breakage caused by excessive fiber bending. Wang et al. noted that the location of filament breakage is hard to determine, and thus fibers are assumed to be constant in length (30 mm in their study) since filaments break randomly and their properties are not uniform.[23] At higher airspeeds (not necessarily turbulent conditions), the fiber tends to align itself perpendicular to the airstream and offers more area for fiber folding and entangling with other fibers.[23] A recommendation to reduce fiber curling and entanglement is to use a die with a slot angle of 60 degrees that aligns with previous studies since air flow at this angle minimizes turbulence.[23] Han et al. note that melt viscosity plays an important role in fiber breakup and recommend that higher viscosity polymers could reduce fiber breakup.[54]

Fiber whipping, also known as the bending instability (or fiber vibration), is characterized by a chaotic motion of the fiber in flight with the possibility of "back-folding" on itself.[47] This motion can occur in a 2D plane for slot dies or in a 3D helical-like motion for spiral dies.[55] Unlike for electrospinning, the whipping motion in melt blowing is an aerodynamic-driven bending instability.

https://doi.org/10.1021/acs.iecr.1c03444
Ind. Eng. Chem. Res. 2022, 61, 65−85

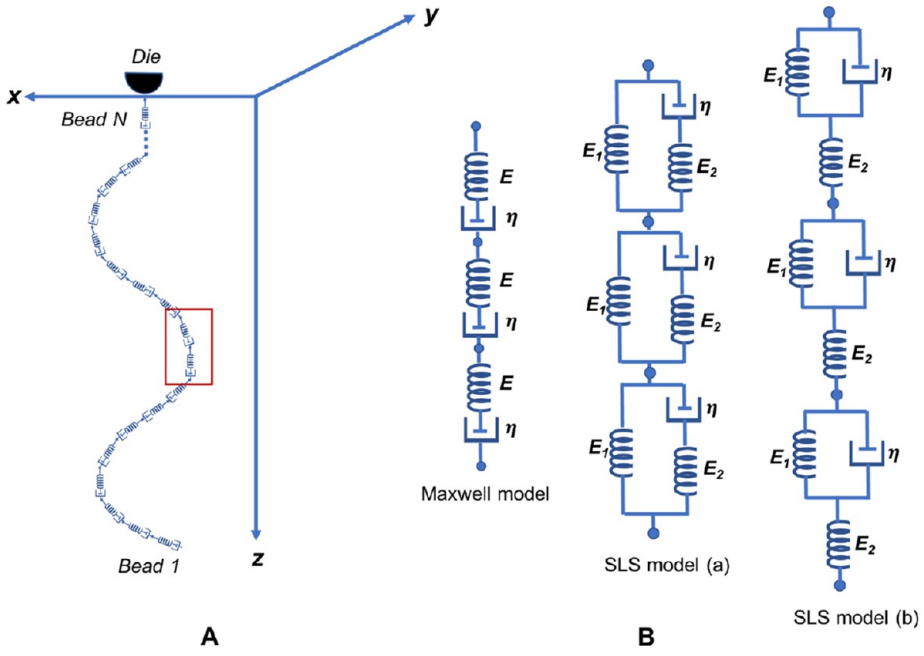

Figure 18. Different spring-mass fiber models.

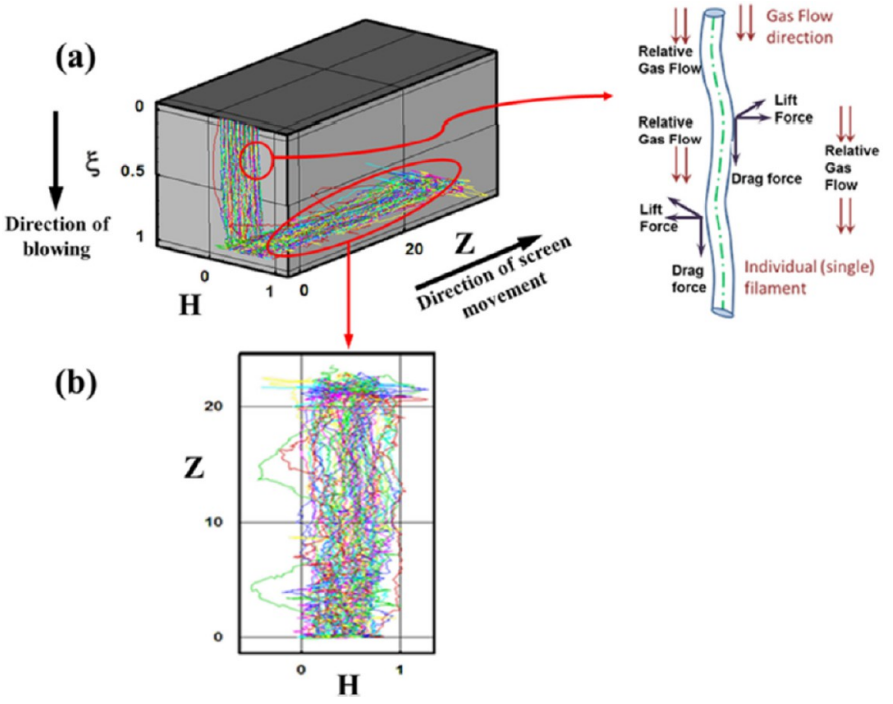

Figure 19. 3D modeling of fiber webs based on touchdown times. Reproduced with permission from ref 8. Copyright 2016 Elsevier.

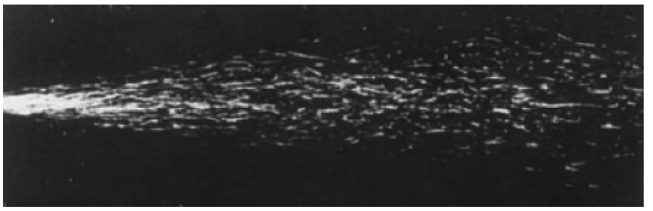

Figure 20. Fiber breakage in the airstream. Reproduced with permission from ref 23. Copyright 2005 American Chemical Society.

This aerodynamic-driven bending instability was proposed by Entov and Yarin,[56] according to which a small disturbance of the polymer filament will be amplified if the air velocity incident on the filament exceeds a critical value. Xie and Zeng experimentally verified using a blunt-edge slot die that for certain processing conditions, the maximum centerline air velocity exceeded the threshold value in a region close to the die exit (<5 cm). This condition induced the whipping motion of the polymer filament as soon as it exited the orifice.[57] Moreover, the authors noted significant turbulence fluctuations

https://doi.org/10.1021/acs.iecr.1c03444
Ind. Eng. Chem. Res. 2022, 61, 65−85

in this region, which could exacerbate the fiber whipping motion.[47,57]

The onset of whipping was further studied by Chung and Kumar, wherein they indicated the role of melt inertia to be dominant over melt rheology in determining fiber shapes.[58] Moreover, the high inlet stream perturbations, strong longitudinal stresses along the fiber axis, decreasing drag forces along the fiber length, and a decreasing centerline velocity further from the inlet play a critical role in the onset of whipping after it exits the die. Fiber whipping typically occurs after the region of fiber attenuation.[8,59] However, after exiting the orifice, although the fiber diameter is too large to undergo any bending motion, it is still susceptible to the growth of minor oscillations along its surface.[42,55,60]

An interesting study by Sun et al. found that for high air velocities (280 m/s), the whipping amplitude increases further from the die, but low air velocities (110 m/s) show a rapid increase in whipping amplitude near the die exit, which then decays rapidly further downstream.[61]

An approach to minimize fiber whipping is to minimize the spread of the air flow field through the use of a solid boundary to guide the fiber and air flow. However, care must be taken to avoid fiber contact with the boundary wall which could lead to clogging.[47,58,60] The use of an annular die can lead to less fiber whipping with a more stable air flow field.[58] Adding an outer-director to a slot die (marked red in Figure 21) can decrease

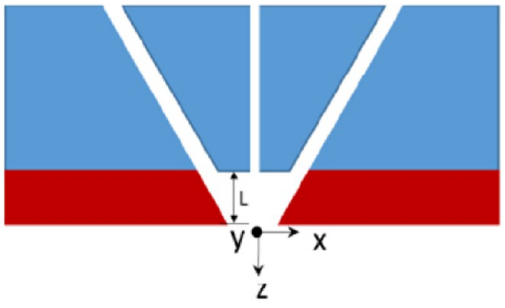

Figure 21. Nozzle (blue) with outer-director (red). Reproduced with permission from ref 60. Copyright 2021 The Authors under Creative Commons CC-BY 4.0, published by MDPI.

air velocity fluctuations, which can suppress fiber oscillations and minimize whipping.[60] If the turbulent nature of fiber whipping can be understood and controlled, it could potentially be used to further attenuate the fibers to smaller diameters.[61]

Verifying Fiber Simulations with Experiments. Some approaches to verify simulation results include qualitatively inspecting the final fiber web or quantifying the fiber diameter and diameter distribution. High-speed imaging techniques are used to observe the fibers in flight for the entire span of the fiber field. Wang et al. observed that limiting the simulation to two initial fiber angles was not enough to accurately produce experimental results.[23] Realistic results require that more computational resources be deployed to model a wider selection of initial fiber angles. While in flight, the fiber diameter and temperature can be measured via high-speed flash photography (1000−5000 frames/s)[31] and infrared imaging.[53] Another in-flight phenomenon that can be captured by photography is fiber vibrational frequencies, which are poorly reproduced in simulations with air turbulence and are often neglected for simplicity.[22]

Combining Fiber Simulations with Air Flow Simulations. The air flow field simulations detailed in the section "Air Flow Simulations" were performed on a standalone basis, i.e., the studies assumed that the presence of the fiber did not affect the air flow distribution or other air flow characteristics. Similarly, predetermined velocity and temperature distributions of airfields (through simulations or experiments) were used as boundary conditions in the simulations of fiber dynamics described in the section "Fiber Simulations". This strategy allowed simulations to be less computationally expensive, but the dynamic interactions of the polymer fiber with the airfield are not captured accurately by this approach.

To the best of our knowledge, the difficult task of simultaneous modeling of fiber and air dynamics during the melt blowing process was first undertaken by Krutka et al., who studied the effect of the presence of fiber on the air flow field using a slot die[30] and an annular die.[29] For the case of a slot die (shown in Figure 22), the presence of the fiber in the airfield reveals more useful information in three dimensions as opposed to one or two dimensions for the standalone cases albeit at increasing computational cost. However, the use of symmetric boundary conditions along $x = 0$ reduces the computational domain. Their results tested the validity of the aforementioned simplified assumption of the negligible effect of fiber on the air flow field and gave better physical insights into the process.

In their work, they used the model developed by Marla and Shambaugh[22] for single fiber dynamics and the RSM for nonisothermal compressible air flow dynamics.[20,25,62] Thus, fiber velocities predicted by the Marla and Shambaugh model[22] were input as user-defined functions in the simulations that set the fiber as a moving boundary, while the predicted z-profiles of the fiber radius were defined as the boundaries of the computational domain. The process was modeled as time-independent with a mean flow of air and polymer, neglecting any fiber oscillations resulting from air turbulence.

The numerical simulation results indicate that the presence of a fiber in the air flow field significantly decreases the recirculation area and reduces the undesirable negative centerline velocity of air close to the die exit. The presence of the fiber reduces the intensity of turbulence (velocity fluctuations) in the air flow field and increases the air velocities for enhanced fiber attenuation at lower energy costs. Moreover, it is instructive to note that performing air flow field simulations in three dimensions in the presence of fiber captures the nonuniformities in air velocity and drag force for fiber attenuation along the radial position on the fiber edge (shown in Figure 23). This could provide further insights into the onset of whipping motion or nonuniformities in fiber diameter. Overall, the presence of the fiber influences the air flow conditions around it, thus better reflecting the melt blowing process.[54]

Similarly, the simulation results for an annular melt blowing die indicate that the presence of a no-slip boundary condition at the air−fiber interface causes a significant reduction in the velocity fluctuations in the air flow field close to the die exit, decreases the size of the recirculation zone (shown in Figure 24), and delays random fiber motion. However, far away from the die exit, the presence of the fiber shows a negligible effect on the fiber or air flow dynamics, and all dynamic variables, including air velocity and turbulence dissipation profiles, become similar.[29,31] Both the above works involving simultaneous modeling of air and fiber flow dynamics were

https://doi.org/10.1021/acs.iecr.1c03444
Ind. Eng. Chem. Res. 2022, 61, 65−85

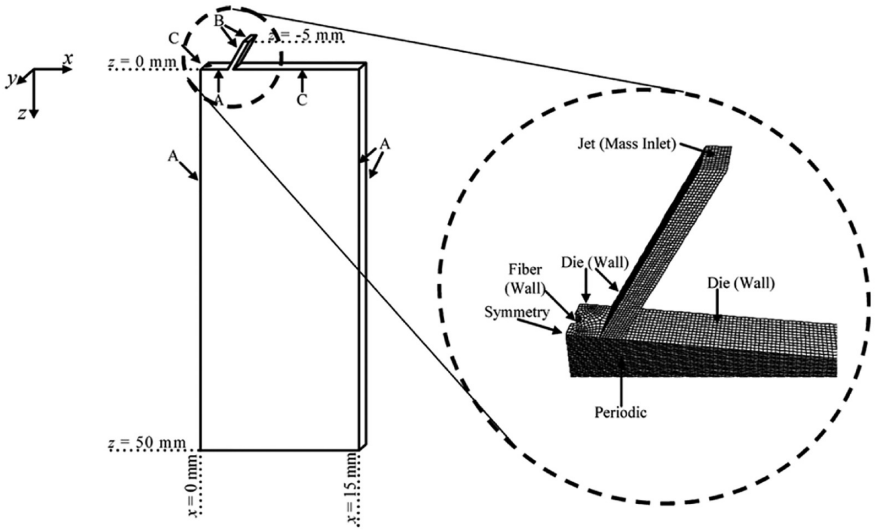

Figure 22. Computational domain used in the air−fiber melt blowing simulations with a magnified region (broken circle) close to the slot die exit. The die face is positioned at $y = 0$ and extends 50 mm in the z-direction. The computational domain also includes the air jet that extends 5 mm above the die face. The $y = 0$ plane corresponds to the center of the domain. The edges A, B, and C are labeled according to the cell sizes: "A" having an average cell edge length of 0.08 mm with a successive ratio of 1.002, "B" having cells with 0.08 mm spacing, and "C" having cell spacing of 0.12 mm. Reproduced with permission from ref 30. Copyright 2008 American Chemical Society.

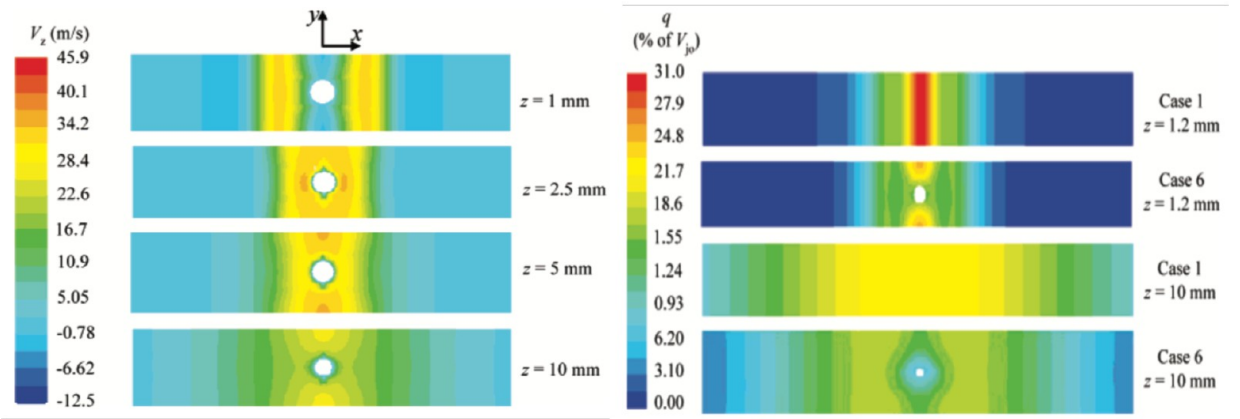

Figure 23. Contour plot of axial velocity (V_z) and turbulence intensity (q, as a percentage of V_{jo}, the nominal velocity at the die face: $q = 1/(3V_{jo})(\overline{u_i u_i})^{0.5}*100\%$) as a function of axial distance (z direction) below the slot die face. Case 1 and case 6 represent the absence and presence of fiber in the air flow field. Reproduced with permission from ref 30. Copyright 2008 American Chemical Society.

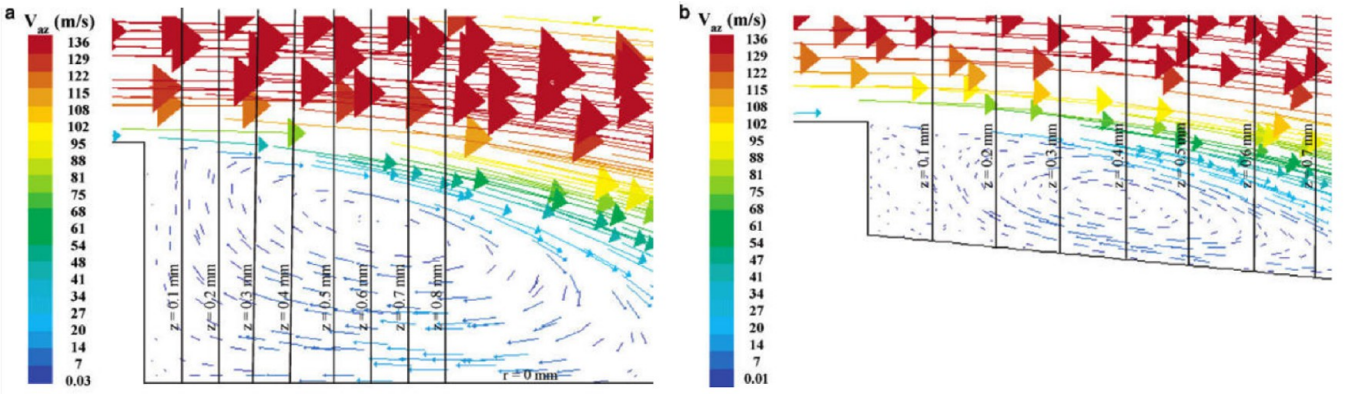

Figure 24. Axial velocity vector plot in the recirculation zone during the melt blowing process in a) the absence of fiber and b) the presence of fiber for the case of annular die. Reproduced with permission from ref 29. Copyright 2007 American Chemical Society.

https://doi.org/10.1021/acs.iecr.1c03444
Ind. Eng. Chem. Res. 2022, 61, 65−85

performed with the momentum ratio between polymer filament and air-jet as an input variable. The developed models could be further enhanced to study the combined effects of varying inlet air temperature, different die geometries, and other processing conditions on final fiber characteristics to optimize the melt blowing process.

Hao et al. used the Level Set Method (LSM) to simulate polymer filament and air velocities during the melt blowing process.[63] LSM is a powerful computational tool for modeling two-phase flow with complex moving boundaries using a fixed mesh.[64] In addition to the general flow dynamic equations described in previous studies, LSM involves solving an additional equation governing the position of the interface between the polymer and air. Using this technique, the authors were able to capture the jet velocity in the direction transverse to the fiber attenuation axis (which is difficult to measure experimentally) within a close agreement to experimentally determined values. Although the model developed was limited to systems with a low Deborah number (elasticity of polymer assumed negligible), it was able to close the gap between experiments and simulations observed in most previous works and was also able to predict suitable processing conditions for achieving desired fiber characteristics.

Polymer Feed Distribution. To produce uniform fibers on a large scale, it becomes necessary to have a feed distribution system capable of maintaining an even mass distribution and a uniform pressure of polymer across the feed area.[65] It is also desirable that the distribution system minimizes pressure losses to save input energy and be designed to minimize clogging while facilitating its cleaning. A metric used to track the effectiveness of the feed distribution is the evenness index (ideal case value is 1) which relies on its geometry and the non-Newtonian material properties but is independent of the polymer viscosity.[65] The performance of the feed distribution system can be studied using CFD simulations with feed distribution geometry and polymer properties as input parameters.

T-Type Feed Distribution. The most basic feed distribution system is the T-type model which is aptly named for its geometry (shown in Figure 25). The liquid

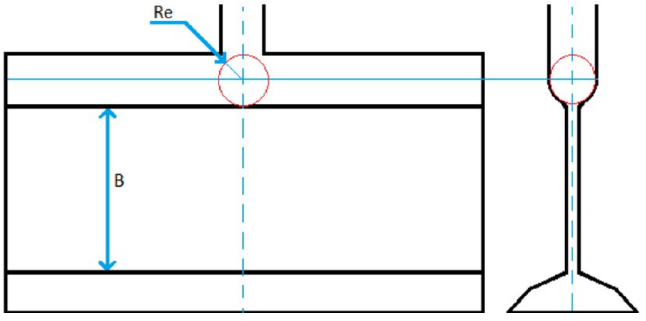

Figure 25. Schematic of a T-type feed distribution system; here B is the land height, also called the height of the regulated area, and R_e is the radius of the inlet.

polymer enters through a single inlet and flows into the manifold area. The thinner regulated area ensures that the polymer spreads evenly until it reaches the die where the polymer chains elongate before entering the airstream. The T-type distribution feed system is no longer used as much given that other geometries offer greater benefits of a more even flow and residence time with minimal drawbacks such as polymer clogging.

Fishtail Feed Distribution. The fishtail model improves upon the T-type model by having the manifold curving downward and a decreasing manifold area further from the inlet. This ensures the liquid polymer is distributed evenly across the width of the die at uniform pressure.[66] Wang et al. found that a 30-degree angle with respect to the horizontal plane and an increased 'land height' (the flat region before the die, i.e., distance 'B' in Figure 26), would ensure a more

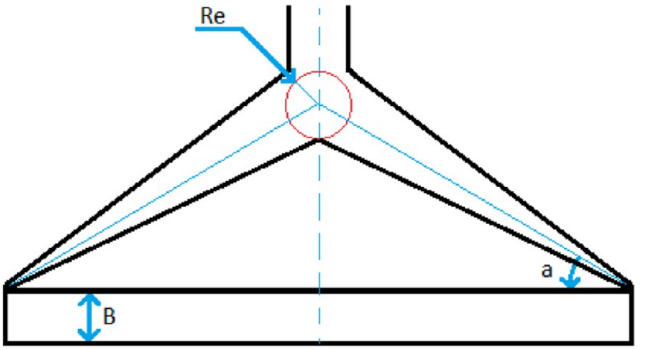

Figure 26. Schematic of a fishtail feed distribution system. Here, B is the land height, a is the angle of the fishtail, and R_e is the radius of the inlet.

uniform polymer flow rate distribution.[66] However, a further increase in land height would lead to more pressure losses requiring more energy to pump the liquid polymer. The simulation results predicting flow rates for different settings are compared to lab experiments which use Laser Doppler Velocimetry (LDV) and Particle Image Velocimetry (PIV) techniques.[66]

Coat-Hanger Feed Distribution. The coat-hanger feed distribution design, most commonly used in industry, combines the manifold area of the T-type and the fan-shaped area of the fishtail type to improve on the drawbacks of previous designs.[65,66] Similar to the fishtail type, the coat-hanger model has a decreasing radius of the manifold at an angle but with a curved geometry as shown in Figure 27. This lessens clogging by reducing the residence time of the polymer in the manifold area and controls the spread of the polymer in an even manner.[65] CFD computations by Yin et al. reveal that

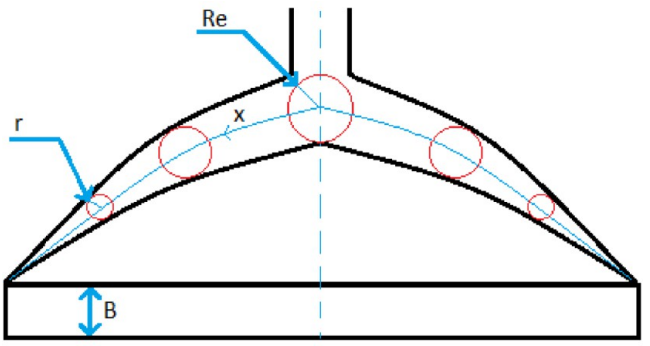

Figure 27. Schematic of a coat-hanger feed distribution system, where B is the land height, and R_e is the radius of the inlet with a decreasing radius r at a distance x along the channel.

https://doi.org/10.1021/acs.iecr.1c03444
Ind. Eng. Chem. Res. 2022, 61, 65−85

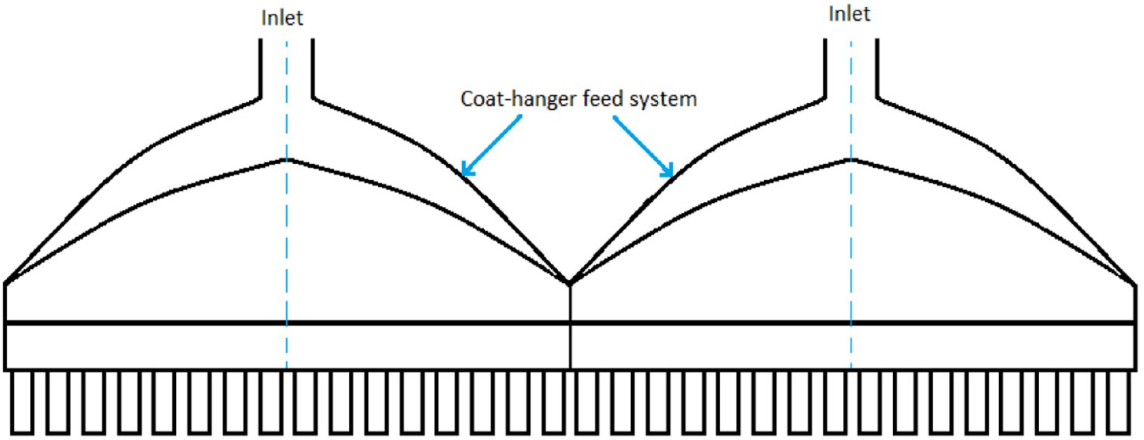

Figure 28. Schematic of a double-width coat-hanger feed distribution system.

the coat-hanger model has a uniform pressure distribution and flow distribution along the exit of the system.[65]

Meng et al. simulated a double-width coat-hanger feed distribution system, having a series of multiple holes in line as shown in Figure 28, that would minimize pressure drop along the die thus lowering energy consumption.[67] Their molten polymer was assumed to be an incompressible and isothermal non-Newtonian fluid with a pure viscous model. The addition of a spinneret plate before the die entrance enforces uniformity of velocity across the die outlet making the double-width feed distribution system a reliable method for uniform melt blowing webs.

MATERIAL PROPERTIES

In previous sections, air and fiber simulations in the melt blowing process were discussed including their combination in determining suitable processing conditions to achieve a certain quality of the final nonwoven systems. Apart from the processing conditions, such as temperature and mass flow rates of air and polymer streams, physical properties of the selected polymer play a critical role in determining the final fiber characteristics like the average diameter and diameter distribution, which in turn determine the pore size and distribution of the nonwoven fiber mat obtained. In this section, an overview of the studies showing the effect of various physical properties like viscoelasticity, viscosity dependence on temperature, and shear-induced crystallization of the polymer feed stream on the final fiber properties is presented.

In the melt blowing process, a wide range of thermoplastic polymers have been used to produce nonwovens. Even though polypropylene (PP) is the most widely used for commercial melt blowing, other polymers such as polyethylene (PE), poly(ethylene terephthalate) (PET), poly(butylene terephthalate) (PBT), and Nylon have been successfully melt blown. Some of these polymers are semicrystalline, while others are amorphous. PS and PMMA have been extensively used in a laboratory setting for research purposes. Ellison et al. summarized the various physical properties that play a role in governing the dynamics of the melt blowing process of such polymers.[14] For example, the extensional viscosity, extensional strain rate, and effect of extensional strain hardening play a major role in the attenuation of polymer fiber and the final fiber characteristics. However, there is significant difficulty in determining the exact experimental values at the fiber extensional strain rates obtained during melt blowing.[8,24]

Another study used simulations and complementary experiments to show that increasing the viscosity significantly increases the average fiber diameter while decreasing the spread of the diameter distribution.[6] Similarly, increasing the elasticity of the feed polymer increases the final fiber diameter while decreasing its standard deviation.[6]

In one of the earliest reports, Uyttendaele and Shambaugh presented a general model for fiber dynamics using a 1D slender jet model based on previous work on melt spinning.[68] Both Newtonian and viscoelastic Phan-Thein Tanner (PTT) constitutive equations were used to represent the components of the stress tensor in the axial and the transverse directions.[22,51] The predictions of fiber diameter, stress-growth, and axial temperature profiles were compared to experimental data for melt blowing of a commercial polypropylene with 35 MFR (melt flow rate). The Newtonian constitutive equation assumes a linear dependence of stress components on velocity gradients, while the PTT model allows the use of a discrete spectrum of relaxation times. The PTT model accounts for the viscoelastic behavior of a polymer in an elongational flow field. The values of parameters describing the viscoelastic properties of the polymer in the PTT model are reported elsewhere.[69]

Uyttendaele et al. found that in the lower range of gas velocities, the Newtonian and the PTT constitutive equations showed excellent agreement with the experiments for the axial variation of the fiber diameter up to a certain point along the fiber axis from the die exit.[68] However, for higher gas velocities, both constitutive equations predict slightly higher diameters compared to experimental values in the entire range of axial distance measured from the die exit. Similarly, the Newtonian and the PTT constitutive models agree well with each other for predicting the axial variation of the stresses along the fiber. The predictions of the various parameters do not depend significantly on the choice of constitutive equations for the stress tensor. One possible explanation for this is the high axial-temperature gradients in melt blowing where temperature dependence of the viscosity becomes the dominant effect.

Given the close predictions of the Newtonian model with the PTT constitutive equations, Uyttendaele and Shambaugh concluded that the changes in the viscoelastic properties of the polymer, such as the shear-thinning parameter, the stress relaxation at high extensional rates typical to commercial melt blowing, and the elastic modulus, do not play a significant role in determining the final fiber properties.[68] The other

https://doi.org/10.1021/acs.iecr.1c03444
Ind. Eng. Chem. Res. 2022, 61, 65−85

constitutive models used to study viscoelastic polymer melts include the Upper Convected Maxwell (UCM) model,[70] the standard linear solid (SLS) model,[53] and the Giesukus model.[71] UCM takes into account the time variation of stress components along the fiber. The SLS model represents the viscoelastic material as a linear combination of springs and dampers which correspond to the elastic and viscous components in the material. Different versions of SLS are used which combine the aspects of the Maxwell model and Kelvin−Voigt model in various combinations.

Although Uyttendaele and Shambaugh concluded that in the range of shear rates studied, the final fiber properties predicted by simulations do not depend on the specific viscoelastic constitutive equation used, they emphasized the importance of temperature dependence of viscosity in the model.[68] Fiber and air simulations show that the fiber temperature drops significantly after exiting the die outlet, and hence there is a significant increase in the viscosity of the polymer fiber. For example, the viscosity of PP decreases by a factor of 3 upon increasing the temperature of the polymer fiber stream by 40 °C, while that of PS decreases almost an order of magnitude on increasing the processing temperature by 100 °C.[14] The temperature dependence of viscosity is given by the William Landau Ferry (WLF) equation which can be used to make the existing model more predictive.[72]

Tan et al. extended the study of Shambaugh et al.[68] to understand how the viscoelasticity of a starting material influences the diameter of melt blown fibers.[6] A 1D slender-jet model was employed where normal stresses of the viscoelastic polymer were evaluated using Newtonian, UCM, and PTT constitutive equations with the fiber whipping motion being neglected. It is instructive to note that the model of Tan et al. assumes isothermal conditions, constant shear stress, and constant length of the fiber attenuation region. These assumptions deviate from the actual melt blowing process, and hence there is only a qualitative agreement of the model predictions with experiments.

Tan et al. studied the final fiber diameter as a function of shear stress and the Deborah number (*De*, defined as the ratio of the longest polymer relaxation time scale to the process time scale).[6] At low shear stresses, the viscoelastic properties do not play a role in determining the fiber diameter. This is in accordance with the observations by Shambaugh et al.[68] for the shear rates studied. However, as the shear rate is increased, higher *De* values predict higher diameter values for both the PTT and the UCM models, thus highlighting the role played by polymer viscoelasticity. In the higher range of shear stress, the diameter decreases steadily with increasing shear stress for the Newtonian case. For the viscoelastic case, the diameter decreases much more slowly with the PTT model and reaches a plateau with the UCM model.

Since Tan et al. modeled a steady-state solution of a single fiber, the influence of viscoelasticity on the fiber diameter distribution cannot be predicted. However, this study provides additional insights into controlling the fiber diameter using the viscoelastic properties of the polymer. The model can be made fully predictive yet computationally tractable by incorporating heat transfer and air flow modeling, in particular, the turbulent nature of air flow to account for the whipping motion observed in experiments.

A more detailed study by Zhou et al. built on the work of Tan et al. by including variable shear stress along the fiber length, as well as heat transfer effects from air flow simulations.[51] Also, the behavior of the Giesekus constitutive model in predicting fiber properties was explored. At low shear stress, the Giesekus model predicts diameters similar to Newtonian and UCM models. At higher shear stress, the Giesekus model predicts fiber diameters between those for the Newtonian and UCM models since the stress predicted by the Giesekus model lies between the Newtonian and UCM models. At very high shear stress, the Giesekus model predictions agree with the Newtonian case. Also, it was concluded that the nonuniform shear stress and the non-isothermal conditions do not change the qualitative behavior of the fiber diameter profiles with shear stress or elasticity. Viscoelasticity leads to higher fiber diameters, more prominently at higher shear stress values.

Zhou et al. also performed linear stability analysis for their melt blowing model to provide deeper insights into the experimental observations by Tan et al. on fiber diameter distribution.[51] They showed that the magnitude of any disturbance amplification along the fiber surface during melt blowing reduces due to viscoelastic effects of the polymer. For sufficiently elastic polymer melts, the disturbances decay faster compared to a Newtonian model. Thus, viscoelasticity gives rise to a narrower fiber diameter distribution.

The other important physical property of the polymer which plays a significant role but adds severe complexity in determining the final melt blown fiber characteristics is the crystallinity of the selected polymer.[50,59] Ziabicki and Lewandowski modified the 1D slender jet model proposed by Uyttendaele and Shambaugh to study fiber dynamics but included the effect of shear-induced crystallization.[7] Their model included an additional equation governing the structure development which takes into account the amorphous orientation and oriented crystallization. Shambaugh et al. adopted a similar model to study the crystallization dynamics in a commercial melt blowing process.[50] Simulations indicate that for a low molecular weight polymer, very little crystallization occurs in the commercial melt blowing process, which is counterintuitive to many experimental results and may require further investigation. However, simulations show significant crystallinity for a higher molecular weight polymer since the spinning speeds are lower and thus have longer exposure to temperatures near the optimum crystallization temperature.

Future Challenges. Nonwovens are an ∼$50 billion market,[15] with melt blowing accounting for a large portion of produced fibers. A radical improvement in simulations would further promote the creation of fibers with specific quality, porosity, surface area, etc. needed in filtration and many other specialized applications. The models developed for melt blowing could be extended to further refine mass production of nanofibers, study the development of other materials, such as thermosets using in situ photopolymerization,[73] or explore unique fiber architectures, such as helical fibers which increase surface area and porosity.[74]

Mathematical models from centrifugal spinning could be adopted for more robust melt blowing modeling, as they capture similar issues, such as air drag, polymer rheological properties, and other forces, to tune the fiber quality and size.[75] The fundamental limit on the smallest achievable size of the fiber along with the suitable processing conditions to attain finer fibers could be investigated further. More rigorous rheological models can be incorporated to study the effect of

https://doi.org/10.1021/acs.iecr.1c03444
Ind. Eng. Chem. Res. 2022, 61, 65−85

polymer rheology and other process variables on fiber size distribution.

The challenges of developing a holistic model for the melt blowing process have been addressed in different areas of research within the field. Using CFD, fiber attenuation is known to be strongly dependent on airspeed, air temperature decay, and the intensity of turbulence. Additional levels of complexity in turbulence modeling are required to accurately capture and control fiber whipping or to investigate multijet die arrangements. Fundamental advances could be made to understand and control other fiber defects in the melt blowing process. The area of feed distribution modeling does not pose a major challenge for simulations, but understanding their performance with novel materials could warrant further investigation.

With considerable research being performed in the field of melt blowing, the ultimate goal should be to develop a unified model to capture all physical processes, from feed distribution to fiber mat collection, for precise control of the final fiber and mat characteristics. With several different models in place, improvements in the die geometry and configurations could be made to control unwanted fiber manufacturing obstacles. Given the large and multiscale parameter space at play, the goal of a unified model may be further out. However, with powerful computational resources and well-placed assumptions, understanding the process as a whole may be an achievable goal which is likely to bear considerable fruit.

AUTHOR INFORMATION

Corresponding Authors

Karen Lozano − *Mechanical Engineering Department, The University of Texas Rio Grande Valley, Edinburg, Texas 78539, United States;* orcid.org/0000-0002-6676-8632; Email: karen.lozano@utrgv.edu

Christopher J. Ellison − *Department of Chemical Engineering and Materials Science, University of Minnesota, Minneapolis, Minnesota 55455, United States;* orcid.org/0000-0002-0393-2941; Email: cellison@umn.edu

Authors

Joseph Schmidt − *Mechanical Engineering Department, The University of Texas Rio Grande Valley, Edinburg, Texas 78539, United States;* Present Address: Department of Physics, The University of Texas at Austin, Austin, TX 78712

Saurabh Shenvi Usgaonkar − *Department of Chemical Engineering and Materials Science, University of Minnesota, Minneapolis, Minnesota 55455, United States*

Satish Kumar − *Department of Chemical Engineering and Materials Science, University of Minnesota, Minneapolis, Minnesota 55455, United States;* orcid.org/0000-0003-0829-6355

Complete contact information is available at: https://pubs.acs.org/10.1021/acs.iecr.1c03444

Author Contributions

[§]J.S. and S.S.U. contributed equally.

Notes

The authors declare no competing financial interest.

ACKNOWLEDGMENTS

This research was supported by the National Science Foundation Partnership for Research and Education in Materials program through grant DMR-2122178. S.S.U. acknowledges partial support through a fellowship awarded by the PPG Foundation.

REFERENCES

(1) Krutka, H. M.; Shambaugh, R. L.; Papavassiliou, D. V. Analysis of multiple jets in the Schwarz melt-blowing die using computational fluid dynamics. *Ind. Eng. Chem. Res.* **2005**, *44*, 8922−8932.

(2) Mukhopadhyay, A.; Sun, J.; Troshko, A.; Prasad, R. O. Modeling and Analysis of Polymer and Air Flow Configurations in Nonwovens Industry; *Proceedings of the Beltwide Cotton Conferences*; Atlanta, GA, USA, 2002.

(3) de Rovère, A.; Shambaugh, R. L. Melt-spun hollow fibers for use in nonwoven structures. *Ind. Eng. Chem. Res.* **2001**, *40*, 176−187.

(4) Yarin, A. L.; Pourdeyhimi, B.; Ramakrishna, S. *Fundamentals and applications of micro-and nanofibers*; Cambridge University Press: 2014; DOI: 10.1017/CBO9781107446830.

(5) Dutton, K. C. Overview and analysis of the meltblown process and parameters. *Journal of Textile and Apparel, Technology and Management* **2008**, *6*, 1.

(6) Tan, D. H.; Zhou, C.; Ellison, C. J.; Kumar, S.; Macosko, C. W.; Bates, F. S. Meltblown fibers: Influence of viscosity and elasticity on diameter distribution. *J. Non-Newtonian Fluid Mech.* **2010**, *165*, 892−900.

(7) Jarecki, L.; Ziabicki, A. Mathematical modelling of the pneumatic melt spinning of isotactic polypropylene, Part II. Dynamic model of melt blowing. *Fibres Text. East. Eur.* **2008**, *16*, 17−24.

(8) Ghosal, A.; Sinha-Ray, S.; Yarin, A. L.; Pourdeyhimi, B. Numerical prediction of the effect of uptake velocity on three-dimensional structure, porosity and permeability of meltblown nonwoven laydown. *Polymer* **2016**, *85*, 19−27.

(9) Lee, Y.; Wadsworth, L. C. Structure and filtration properties of melt blown polypropylene webs. *Polym. Eng. Sci.* **1990**, *30*, 1413−1419.

(10) Bresee, R. R.; Qureshi, U. A. Influence of processing conditions on melt blown web structure: Part 1−DCD. *Int. Nonwovens J.* **2004**, *os13*, 1558925004os-13.

(11) Yarin, A. L.; Sinha-Ray, S.; Pourdeyhimi, B. Meltblowing: Multiple polymer jets and fiber-size distribution and lay-down patterns. *Polymer* **2011**, *52*, 2929−2938.

(12) Tan, D. H.; Herman, P. K.; Janakiraman, A.; Bates, F. S.; Kumar, S.; Macosko, C. W. Influence of Laval nozzles on the air flow field in melt blowing apparatus. *Chem. Eng. Sci.* **2012**, *80*, 342−348.

(13) Lee, Y.; Wadsworth, L. C. Structure and filtration properties of melt blown polypropylene webs. *Polym. Eng. Sci.* **1990**, *30*, 1413−1419.

(14) Ellison, C. J.; Phatak, A.; Giles, D. W.; Macosko, C. W.; Bates, F. S. Melt blown nanofibers: Fiber diameter distributions and onset of fiber breakup. *Polymer* **2007**, *48*, 3306−3316.

(15) Russell, S. J. *Handbook of nonwovens*; 2007.

(16) Drabek, J.; Zatloukal, M. Meltblown technology for production of polymeric microfibers/nanofibers: A review. *Phys. Fluids* **2019**, *31*, 091301.

(17) Drábek, B. J. *Applied Rheology for Production of Polymeric Nanofibers*, Ph.D. Thesis, Tomas Bata University in Zlín, 2013.

(18) Marla, V. T.; Shambaugh, R. L. Modeling of the melt blowing performance of slot dies. *Ind. Eng. Chem. Res.* **2004**, *43*, 2789−2797.

(19) Wang, Y.; Wang, X. Investigation on a new annular melt-blowing die using numerical simulation. *Ind. Eng. Chem. Res.* **2013**, *52*, 4597−4605.

(20) Krutka, H. M.; Shambaugh, R. L.; Papavassiliou, D. V. Effects of die geometry on the flow field of the melt-blowing process. *Ind. Eng. Chem. Res.* **2003**, *42*, 5541−5553.

(21) Sun, Y. F.; Liu, B. W.; Wang, X. H.; Zeng, Y. C. Air-flow field of the melt-blowing slot die via numerical simulation and multiobjective genetic algorithms. *J. Appl. Polym. Sci.* **2011**, *122*, 3520−3527.
(22) Marla, V. T.; Shambaugh, R. L. Three-dimensional model of the melt-blowing process. *Ind. Eng. Chem. Res.* **2003**, *42*, 6993−7005.
(23) Wang, X.; Ke, Q. Computational simulation of the fiber movement in the melt-blowing process. *Ind. Eng. Chem. Res.* **2005**, *44*, 3912−3917.
(24) Hassan, M. A.; Anantharamaiah, N.; Khan, S. A.; Pourdeyhimi, B. Computational fluid dynamics simulations and experiments of meltblown fibrous media: new die designs to enhance fiber attenuation and filtration quality. *Ind. Eng. Chem. Res.* **2016**, *55*, 2049−2058.
(25) Krutka, H. M.; Shambaugh, R. L.; Papavassiliou, D. V. Analysis of a melt-blowing die: Comparison of CFD and experiments. *Ind. Eng. Chem. Res.* **2002**, *41*, 5125−5138.
(26) Chen, T.; Zhang, C.; Chen, X.; Li, L. Numerical computation of the fiber diameter of melt blown nonwovens produced by the inset die. *J. Appl. Polym. Sci.* **2009**, *111*, 1775−1779.
(27) Zachara, A.; Lewandowski, Z. Mathematical modelling of pneumatic melt spinning of isotactic polypropylene, Part I: Modelling of the air jet dynamics. *FIBRES & TEXTILES in Eastern Europe* **2008**, *8*, 10.
(28) Wu, L.; Huang, D.; Chen, T. Modeling the nanofiber fabrication with the melt blowing annular die. *Rev. Mater.* **2014**, *19*, 377−381.
(29) Krutka, H. M.; Shambaugh, R. L.; Papavassiliou, D. V. Effects of the polymer fiber on the flow field from an annular melt-blowing die. *Ind. Eng. Chem. Res.* **2007**, *46*, 655−666.
(30) Krutka, H. M.; Shambaugh, R. L.; Papavassiliou, D. V. Effects of the polymer fiber on the flow field from a slot melt blowing die. *Ind. Eng. Chem. Res.* **2008**, *47*, 935−945.
(31) Hao, X.; Zeng, Y. A review on the studies of air flow field and fiber formation process during melt blowing. *Ind. Eng. Chem. Res.* **2019**, *58*, 11624−11637.
(32) Moore, E. M.; Shambaugh, R. L.; Papavassiliou, D. V. Analysis of isothermal annular jets: Comparison of computational fluid dynamics and experimental data. *J. Appl. Polym. Sci.* **2004**, *94*, 909−922.
(33) Majumdar, B.; Shambaugh, R. L. Velocity and temperature fields of annular jets. *Ind. Eng. Chem. Res.* **1991**, *30*, 1300−1306.
(34) Uyttendaele, M. A. J.; Shambaugh, R. L. The flow field of annular jets at moderate Reynolds numbers. *Ind. Eng. Chem. Res.* **1989**, *28*, 1735−1740.
(35) Launder, B. E.; Reece, G. J.; Rodi, W. Progress in the development of a Reynolds-stress turbulence closure. *J. Fluid Mech.* **1975**, *68*, 537−566.
(36) Durbin, P. A.; Reif, B. A. P. *Statistical theory and modeling for turbulent flows*; John Wiley & Sons: 2011.
(37) Lai, J. C. S.; Nasr, A. Two parallel plane jets: comparison of the performance of three turbulence models. *Proc. Inst. Mech. Eng., Part G* **1998**, *212*, 379−391.
(38) Xie, S.; Han, W.; Jiang, G.; Chen, C. Turbulent air flow field in slot-die melt blowing for manufacturing microfibrous nonwoven materials. *J. Mater. Sci.* **2018**, *53*, 6991−7003.
(39) Xie, S.; Han, W.; Jiang, G. Three dimensional numerical simulation for air flow field in melt blowing. *J. Phys.: Conf. Ser.* **2017**, *916*, 012044.
(40) Krutka, H. M.; Shambaugh, R. L.; Papavassiliou, D. V. Using computational fluid dynamics to simulate flow fields from various melt blowing dies. *Int. Nonwovens J.* **2005**, *os-14*, 1558925005os-14.
(41) Krutka, H. M.; Shambaugh, R. L.; Papavassiliou, D. V. Analysis of the temperature field from multiple jets in the Schwarz melt blowing die using computational fluid dynamics. *Ind. Eng. Chem. Res.* **2006**, *45*, 5098−5109.
(42) Yarin, A. L.; Sinha-Ray, S.; Pourdeyhimi, B. Meltblowing: II-linear and nonlinear waves on viscoelastic polymer jets. *J. Appl. Phys.* **2010**, *108*, 034913.
(43) Chelikani, S.; Sparrow, E. M. Numerical simulations of plane-wall coanda effects for control of fiber trajectories in the melt-blown process. *Ind. Eng. Chem. Res.* **2013**, *52*, 11639−11645.
(44) Harpham, A. S.; Shambaugh, R. L. Flow field of practical dual rectangular jets. *Ind. Eng. Chem. Res.* **1996**, *35*, 3776−3781.
(45) Harpham, A. S.; Shambaugh, R. L. Velocity and temperature fields of dual rectangular jets. *Ind. Eng. Chem. Res.* **1997**, *36*, 3937−3943.
(46) Yin, H.; Yan, Z.; Ko, W.; Bresee, R. R. Fundamental description of the melt blowing process. *Int. Nonwovens J.* **2000**, *os-9*, 1558925000OS-90.
(47) Xie, S.; Zeng, Y. Turbulent air flow field and fiber whipping motion in the melt blowing process: experimental study. *Ind. Eng. Chem. Res.* **2012**, *51*, 5346−5352.
(48) Yang, Y.; Zeng, Y. Simultaneous Measurement in Non-isothermal Melt-Blowing Airflow Field: Time-Averaged and Turbulent Characteristics. *Ind. Eng. Chem. Res.* **2020**, *59*, 10664−10672.
(49) Xie, S.; Jiang, G.; Ye, B.; Shentu, B. Particle Image Velocimetry (PIV) investigation of the turbulent airflow in slot-die melt blowing. *Polymers* **2020**, *12*, 279.
(50) Shambaugh, B. R.; Papavassiliou, D. V.; Shambaugh, R. L. Next-generation modeling of melt blowing. *Ind. Eng. Chem. Res.* **2011**, *50*, 12233−12245.
(51) Zhou, C.; Tan, D. H.; Janakiraman, A. P.; Kumar, S. Modeling the melt blowing of viscoelastic materials. *Chem. Eng. Sci.* **2011**, *66*, 4172−4183.
(52) Zeng, Y. C.; Sun, Y. F.; Wang, X. H. Numerical approach to modeling fiber motion during melt blowing. *J. Appl. Polym. Sci.* **2011**, *119*, 2112−2123.
(53) Han, W.; Wang, X. Modeling melt blowing fiber with different polymer constitutive equations. *Fibers Polym.* **2016**, *17*, 74−79.
(54) Han, W.; Bhat, G. S.; Wang, X. Investigation of nanofiber breakup in the melt-blowing process. *Ind. Eng. Chem. Res.* **2016**, *55*, 3150−3156.
(55) Xie, S.; Zheng, Y.; Zeng, Y. Influence of die geometry on fiber motion and fiber attenuation in the melt-blowing process. *Ind. Eng. Chem. Res.* **2014**, *53*, 12866−12871.
(56) Entov, V. M.; Yarin, A. L. The dynamics of thin liquid jets in air. *J. Fluid Mech.* **1984**, *140*, 91−111.
(57) Xie, S.; Zeng, Y. Online measurement of fiber whipping in the melt-blowing process. *Ind. Eng. Chem. Res.* **2013**, *52*, 2116−2122.
(58) Chung, C.; Kumar, S. Onset of whipping in the melt blowing process. *J. Non-Newtonian Fluid Mech.* **2013**, *192*, 37−47.
(59) Jarecki, L.; Lewandowski, Z. Mathematical modelling of the pneumatic melt spinning of isotactic polypropylene, Part III. Computations of the process dynamics. *Fibres Textiles Eastern Eur.* **2009**, *17*, 75−80.
(60) Yang, Y.; Zeng, Y. Measurement and Comparison of Melt-Blowing Airflow Fields: Nozzle Modifications to Reduce Turbulence and Fibre Whipping. *Polymers* **2021**, *13*, 719.
(61) Sun, Y.; Zeng, Y.; Wang, X. Three-dimensional model of whipping motion in the processing of microfibers. *Ind. Eng. Chem. Res.* **2011**, *50*, 1099−1109.
(62) Krutka, H. M.; Shambaugh, R. L.; Papavassiliou, D. V. Effects of temperature and geometry on the flow field of the melt blowing process. *Ind. Eng. Chem. Res.* **2004**, *43*, 4199−4210.
(63) Hao, X.; Huang, H.; Zeng, Y. Simulation of jet velocity in the melt-blowing process using the coupled air−polymer model. *Text. Res. J.* **2019**, *89*, 3221−3233.
(64) Lan, W.; Li, S.; Wang, Y.; Luo, G. CFD simulation of droplet formation in microchannels by a modified level set method. *Ind. Eng. Chem. Res.* **2014**, *53*, 4913−4921.
(65) Yin, M. F.; Li, X. Q.; Gong, H. A Design for Spinning Die Channel of Melt-blown Nonwoven Fabric. *Appl. Mech. Mater.* **2011**, *66*, 922−926.
(66) Wang, X.; Chen, T.; Huang, X. Simulation of the polymeric fluid flow in the feed distributor of melt blowing process. *J. Appl. Polym. Sci.* **2006**, *101*, 1570−1574.

https://doi.org/10.1021/acs.iecr.1c03444
Ind. Eng. Chem. Res. 2022, 61, 65−85

(67) Meng, K.; Wang, X. Numerical simulation and analysis of fluid flow in double melt-blown die. *Text. Res. J.* **2013**, *83*, 249−255.
(68) Uyttendaele, M. A. J.; Shambaugh, R. L. Melt blowing: general equation development and experimental verification. *AIChE J.* **1990**, *36*, 175−186.
(69) Phan-Thien, N. A nonlinear network viscoelastic model. *J. Rheol.* **1978**, *22*, 259−283.
(70) Macosko, C. W. *Rheology: Principles, Measurements, and Applications*; 1994.
(71) Giesekus, H. A simple constitutive equation for polymer fluids based on the concept of deformation-dependent tensorial mobility. *J. Non-Newtonian Fluid Mech.* **1982**, *11*, 69−109.
(72) Hiemenz, P. C.; Lodge, T. P. *Polymer Chemistry*; CRC Press: 2007.
(73) Banerji, A.; Jin, K.; Liu, K.; Mahanthappa, M. K.; Ellison, C. J. Cross-Linked Nonwoven Fibers by Room-Temperature Cure Blowing and in Situ Photopolymerization. *Macromolecules* **2019**, *52*, 6662−6672.
(74) Li, H.; Huang, H.; Meng, X.; Zeng, Y. Fabrication of helical microfibers from melt blown polymer blends. *J. Polym. Sci., Part B: Polym. Phys.* **2018**, *56*, 970−977.
(75) Noroozi, S.; Arne, W.; Larson, R. G.; Taghavi, S. M. A comprehensive mathematical model for nanofibre formation in centrifugal spinning methods. *J. Fluid Mech.* **2020**, *892*, 892.
(76) Eggenspieler, G. *ANSYS presentation*; 2011; p 4.

https://doi.org/10.1021/acs.iecr.1c03444
Ind. Eng. Chem. Res. 2022, 61, 65−85